Int J Earth Sci (Geol Rundsch) (2016) 105:1307–1327
DOI 10.1007/s00531-015-1250-7

ORIGINAL PAPER

Early Paleozoic magmatic history of central Inner Mongolia, China: implications for the tectonic evolution of the Southeast Central Asian Orogenic Belt

Chen Wu[1] · Changfeng Liu[2,3] · Yan Zhu[2] · Zhiguang Zhou[1] · Tian Jiang[4] · Wencan Liu[2] · Hongying Li[1] · Chu Wu[5] · Baoying Ye[2]

Received: 1 July 2015 / Accepted: 17 September 2015 / Published online: 6 October 2015

Abstract To provide insights into the Early Paleozoic tectonic evolution of the southern portion of the long-lived Central Asian Orogenic Belt, we have conducted major and trace element analyses and zircon U–Pb dating of granitoid samples from central Inner Mongolia. Our study area covers three pre-Mesozoic tectonic units from north to south: the Wenduermiao subduction–accretionary complex, the Bainaimiao magmatic belt, and the northern margin of the North China craton. Our new geochronological and geochemical data show the temporal and genetic relationships between the three tectonic units. Accordingly, we suggest that the Wenduermiao subduction–accretionary complex developed in the Middle Cambrian–Late Silurian (509–421 Ma), comprising of coeval oceanic crust, arc magmatism, and forearc deposits. The Bainaimiao continental arc was developed during the Late Cambrian to Early Silurian (501–437 Ma), which superposed on the basement with the affinity of the North China craton. The back-arc basin opened prior to Early Silurian and lasted to the Late Silurian, which is slightly younger than Bainaimiao island arc. The Wenduermiao Ocean, between the Wenduermiao subduction–accretionary complex and the Bainaimiao continental arc, existed in Early Paleozoic.

Keywords Early Paleozoic · Magmatic history · Tectonic evolution · Central Asian Orogenic Belt · Inner Mongolia

Introduction

In the context of plate tectonics, a complete convergent margin develops with a genetically linked accretionary prism (i.e., a subduction–accretionary complex), forearc with a suprasubduction zone ophiolite, magmatic arc

✉ Chen Wu
wuchenlovegeology@gmail.com; whdx19881224@126.com

Changfeng Liu
nose010@sohu.com

Yan Zhu
zhuyan@cugb.edu.cn

Zhiguang Zhou
zhouzhg@cugb.edu.cn

Tian Jiang
jiangtian71@gmail.com

Wencan Liu
liuwenc@cugb.edu.cn

Hongying Li
lihy@cugb.edu.cn

Chu Wu
wuchu12345@163.com

Baoying Ye
yebaoying@cugb.edu.cn

[1] School of Earth Science and Resources, China University of Geosciences (Beijing), Beijing 100083, China

[2] Institute of Geological Survey, China University of Geosciences (Beijing), Beijing 100083, China

[3] Inner Mongolia Mining Co Ltd., Hohhot 010020, China

[4] College of Zijin Mining, Fuzhou University, Fuzhou 350108, China

[5] School of Water Resources and Environment, China University of Geosciences (Beijing), Beijing 100083, China

(either intra-oceanic or continental), and back-arc basin (Pearce et al. 1984; Stern 2002, 2004). Not all convergent margins have accretionary prisms, only the ones that formed near continents (Stern 2002, 2004). In addition to subduction-related magmatism playing a key role in the development of the convergent margin (Stern 2002, 2004), granitoid batholiths at convergent continental margins are thought to represent crust generated by interaction of mantle-derived magmas and preexisting continental crust (Zhang et al. 2009b). The Central Asian Orogenic Belt (CAOB) was responsible for Phanerozoic juvenile crustal growth (Sengör et al. 1993; Jahn et al. 2004; Windley et al. 2007; Xiao et al. 2003, 2009, 2010; Li et al. 2014), and this large and complex accretionary collage located between the Siberian craton to the north and the North China craton to the south (Fig. 1, inset). The southeastern CAOB in Inner Mongolia of northeastern China formed mainly in the Paleozoic due to the consumption of the Paleo-Asian oceanic basins and accompanying accretion of oceanic plate sediments, oceanic crust, including oceanic islands, forearc and back-arc basins, and magmatic arcs (Xiao et al. 2003; De Jong et al. 2006; Windley et al. 2007; Li et al. 2014). The tectonic evolution of the regional was characterized by bivergent subductions below the southern active margin of the Siberia craton and the northern margins of the North China craton (Xiao et al. 2003, 2009). However, the tectonic evolution style of the southeastern CAOB has been controversial, leading to several competing models (Xiao et al. 2010). Specifically, the following hypotheses have been proposed specifically to evolution of the southeastern CAOB in the northeast China: (1) multiple terrane amalgamation model (Xiao et al. 2003; Windley et al. 2007; Hsü and Chen 1999); (2) oroclinal bending and strike-slip faulting model (Sengör et al. 1993; Von Raumer et al. 2003; Wang et al. 2007; Levashova et al. 2009); and (3) Caledonian composite continent model (Kheraskova et al. 2003). Also, there is still much controversy concerning the timing of the final phase of amalgamation along the northern margin of the North China craton and the southern margin of the Siberian craton, and proposals range from the Ordovician–Silurian, through Devonian–Early Carboniferous, to Permian–Triassic (Sengör et al. 1993; Jian et al. 2008, 2010; Xiao et al. 2003, 2009, 2010; Li et al. 2014).

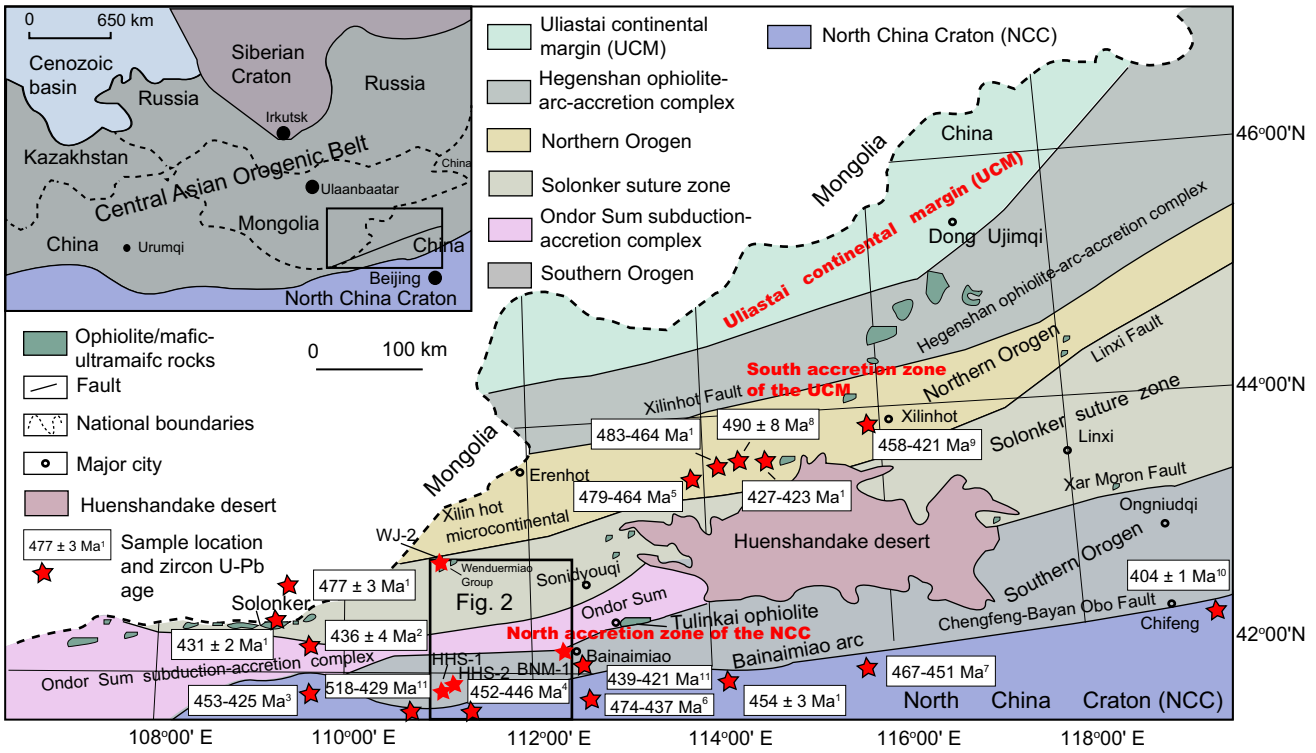

Fig. 1 Sketch map of the geology in the southern Central Asian Orogenic Belt, modified from Jian et al. (2008) based on our own observations showing the Solonker suture zone separating the northern and southern Paleozoic orogens. The *black box* shows the location of the study area. Zircon U–Pb data from (1) Jian et al. (2008); (2) Miao et al. (2007); (3) Xu et al. (2013); (4) Zhang and Jian (2008); (5) Shi et al. (2005); (6) Zhang et al. (2013); (7) Liu et al. (2003); (8) Chen et al. (2000); (9) Ge et al. (2011); (10) Liu et al. (2009); (11) Zhang et al. (2014)

Phanerozoic granites are widespread throughout northeastern China (Wu et al. 2002) and most of which contain a large proportion of juvenile crustal material (Kröner et al. 2014). The Phanerozoic was an extensive period of new crustal growth (CITATION; cf. Kröner et al. 2014). So, systematic isotopic and petrogenetic studies of all the Phanerozoic granitic intrusions in NE China are essential to constrain the global crustal growth. The age of these granitoids ranges from Neoarchean to Early Mesozoic. The exposed Neoarchean basement in the northern part of the North China craton includes major crustal building TTG (tonalite–trondhjemite–granodiorite) rocks, high K granite, and variably deformed diorite, which is characterized by major crustal growth and recycling tectonothermal events at ~2.5 Ga. (Zhou et al. 2009; Zhai and Santosh 2011; Liu et al. 2014). Zhang et al. (2009a) reported that during 1.85–1.80 Ga Paleoproterozoic high-pressure (HP) and high to ultrahigh temperature (HT–UHT) high K granites are related to Paleoproterozoic rifting–subduction–accretion–collision tectonics and subsequent high-grade granulite facies metamorphism–granitoid magmatism during ca. 2.0–1.82 Ga in the North China craton. These Proterozoic granitic batholiths were intruded by Permian granitoids (Zhang et al. 2009c). The Middle Proterozoic–Neoproterozoic Bayan Obo Group strata unconformably overlie the Precambrian granitic batholiths. Early Paleozoic calc-alkaline granitoids (508–454 Ma) were formed in processes of the Paleo-Asian Ocean (Liu et al. 2014; Zhou et al. 2009). Carboniferous–Early Permian (331–299 Ma) are composed of variably deformed diorite, quartz diorite, and gabbro with low K calc-alkaline and alkaline geochemical affinity, which are related to the subduction of the Paleo-Asian Ocean underneath North China during a major subduction-related orogenic period (Liu et al. 2014). However, the Middle–Late Permian granitoids (271–253 Ma), granodiorite, syenogranite, and adamellite, are related to the collision between the Siberia Plate and the North China craton (Liu et al. 2014). The Triassic granitoids (250–224 Ma) might be related to the extensive post-collisional magmatism (Liu et al. 2014). In contrast to the well-studied Late Paleozoic–Mesozoic granitoids in northeastern China, there are no systematic investigations of the Early Paleozoic granitoids in central Inner Mongolia, which hindered testing of the aforementioned competing models and hypotheses for the evolution history in eastern Asia. Previous researchers reported some ages in the southeastern CAOB (Jian et al. 2008; Miao et al. 2007; Xu et al. 2013; Zhang and Jian 2008; Shi et al. 2005; Zhang et al. 2013, 2014; Liu et al. 2003, 2009; Chen et al. 2000; Ge et al. 2011) (Fig. 1); the variations on evolution phase time reflect an incomplete record of isotopic ages and different interpretations of the geological environments of key tectonic units. In order to better test these competing hypotheses, we conducted a reconnaissance investigation of Early Paleozoic granitoids in the Siziwangqi region of central Inner Mongolia. Our work includes zircon U–Pb dating and geochemical analysis of the Early Paleozoic granitoids (location information is given in Table 1) from this region (Fig. 2). Major elements, trace elements, and U–Pb zircon age data of granitoids are used to constrain the petrogenesis of these granitoids in the context of understanding the evolution of the central Inner Mongolia, which also helps understand the evolution of the Paleo-Asian system and mechanisms of the crust growth in response to subduction–collision.

Geological setting

Regional and local geology

The southeastern section of the CAOB is characterized by east-northeast trending tectonic units, consisting of ophiolites, arcs, accretionary wedges and associated volcanosedimentary rocks that were assembled during the final Late Paleozoic–Early Mesozoic closure of the Paleo-Asian Ocean (Sengör et al. 1993; Ye et al. 1994; Xiao et al. 2010). The study region can be divided into three domains, from north to south (Fig. 1): the accretionary zone between the Solonker suture and the Uliastai continental margin, the Solonker suture zone, and the southern accretionary zone between the North China craton and the Solonker suture (Xiao et al. 2003, 2009; Xu et al. 2013). The southern accretionary zone is characterized by the Middle Ordovician to Early Silurian Ondor Sum subduction–accretionary complex (De Jong et al. 2006; Jian et al. 2008, 2010) and the south orogen. The northern accretionary zone extends southward from the Uliastai continental margin (Xiao et al. 2003, 2009) that was active from Devonian to Carboniferous, through the Hegenshan ophiolite–arc–accretion complex to the Late Carboniferous northern orogen. Termination of the subduction of the Paleo-Asian Ocean was followed by the collision of two opposing active continental margins, leading to the formation of the Solonker suture (Xiao et al. 2003, 2009; Xu et al. 2013). Available age constraints suggest that the Phanerozoic granitic rocks in NE China were mainly formed during the Mesozoic, ranging in age from 230 to 120 Ma, and minor Paleozoic granitic magmatism is mainly distributed in western Inner Mongolia (Wu et al. 2000, 2002, 2003a, b, 2014, 2015; Liu et al. 2014). The CAOB of northeastern China involved the Paleozoic collision and amalgamation of several Precambrian microcontinents. The southeastern CAOB was formed by the concurrent two-way oceanic subduction toward opposing continental margins, a typical arc–trench complex in the south and a product of ridge trench interaction in the north (Sengör et al. 1993; Xiao

Table 1 Major and trace elements for the plutonic rocks from this study

Samples	HHS1	HHS2	BNM-1	WJ-2
Major element (wt%)				
SiO_2	64.89	64.63	58.34	58.55
Al_2O_3	18.21	18.1	18.23	16.42
CaO	0.15	0.14	3.48	2.25
Fe_2O_3	0.03	0.07	0.62	0.91
FeO	0.4	0.9	4.78	7.19
K_2O	13.56	13.21	1.24	1.93
MgO	0.08	0.08	2.06	5.08
MnO	0.01	0.01	0.1	0.12
Na_2O	1.9	1.99	5.04	1.44
P_2O_5	0.01	0.02	0.24	0.09
TiO_2	0.05	0.1	0.5	0.89
CO_2	0.05	0.04	2.49	0.65
H_2O^+	0.18	0.12	2.3	3.82
LOI	0.15	0.19	4.17	3.71
Total	99.52	99.41	99.42	99.34
A/CNK	1.013	1.005	1.14	1.92
Mg#	25.4	13.1	41.21	53.54
Trace element (ppm)				
Th	2.54	0.75	7.86	4.13
U	0.36	0.33	1.47	1.24
Cs	0.21	0.31	3.93	2.59
Sc	0.4	0.53	10.9	26
Rb	114	124	28.8	74
Sr	99.9	130	682	169
Ba	281	271	898	376
Zr	45.3	41.9	114	115
Nb	15.3	20.1	8.85	8.34
Ta	0.13	0.12	0.62	0.73
Hf	1.29	1.16	3.31	3.54
Pb	14.2	7.68	12.1	6.91
V	13.5	44.6	123	197
Cr	2.75	4.57	51	142
Co	0.73	1.56	13.9	22.9
Ni	3.21	7.4	24	53.4
Cu	8.65	4.97	6.28	21
Zn	2.89	7.45	98.3	103
Ga	33	34.1	18.7	20.3
La	3.93	3.85	33.6	16.7
Ce	8.19	8.04	56.7	33
Pr	1.02	1.04	7.26	3.97
Nd	3.46	3.67	26.6	14.7
Sm	0.48	0.48	4.27	2.77
Eu	0.13	0.14	1.26	1.22
Gd	0.32	0.41	3.62	2.72
Tb	0.05	0.05	0.49	0.44
Dy	0.18	0.26	2.56	2.71
Ho	0.05	0.05	0.53	0.61
Er	0.12	0.12	1.49	1.86
Tm	0.05	0.05	0.23	0.32
Yb	0.12	0.13	1.56	2.14
Lu	0.05	0.05	0.24	0.35
Y	1.08	1.27	13.7	15.8
$(La/Yb)_N$	21.24	23.49	15.45	5.6
δEu	0.32	0.33	0.32	0.44

et al. 2003; Jian et al. 2008; Liu et al. 2012). The Solonker suture zone records the terminal evolution of the Paleo-Asian Ocean in Inner Mongolia and tectonically separates the southern and northern orogenic belts (Fig. 1; Sengör et al. 1993; Xiao et al. 2003). Jian et al. (2008) suggest that the Early Paleozoic rocks on the southern side of the Solonker suture formed in an Indonesian-type archipelago off the margin of eastern Gondwana, whereas the Early Paleozoic rocks on the northern side of the Solonker suture formed along the southern margin of the growing CAOB. Their convergence during Late Paleozoic led to the collision and the formation of the Solonker suture at ca. 250 Ma (Jian et al. 2008; Liu et al. 2012, 2014). The magmatic rocks of the XilinHot microcontinental are exposed discontinuously along the northern margin of the Lixin Fault (Fig. 1), the northern boundary of the Solonker. The major tectonic units of the southern orogen include the Wenduermiao subduction complex, Tulinkai ophiolite, and Bainaimiao island arc. The Wenduermiao subductionary complex and the Tulinkai ophiolite are parts of the Ondor Sum subduction–accretionary complex (Fig. 1) that comprises turbidites, olistostrome mélanges, and blueschists (Hu et al. 1987, 1990; Xiao et al. 2003; Jian et al. 2008, 2010). The Bainaimiao island arc is in fault contact with North China craton (Fig. 1).

The North China craton is one of the largest cratons in eastern Eurasia, and its major tectonic structures are truncated by younger orogenic belts at the craton margins, covering an area of over 300,000 km^2 and preserving the record of a long and complex crustal evolution and stabilization history, offering an excellent case to evaluate subduction–accretionary and collisional tectonics in the Precambrian Earth (Song et al. 1996; Zhai and Santosh 2011). Five major tectonic cycles have been identified from the North China craton as follows: (1) Neoarchean crustal growth and stabilization, (2) Paleoproterozoic rifting–subduction–accretion–collision, (3) Late Paleoproterozoic–Neoproterozoic multistage rifting, (4) Paleozoic orogene is at the margins of the craton, and (5) Mesozoic extensional tectonics associated with lithospheric thinning and decratonization (Zhai and Santosh 2011).

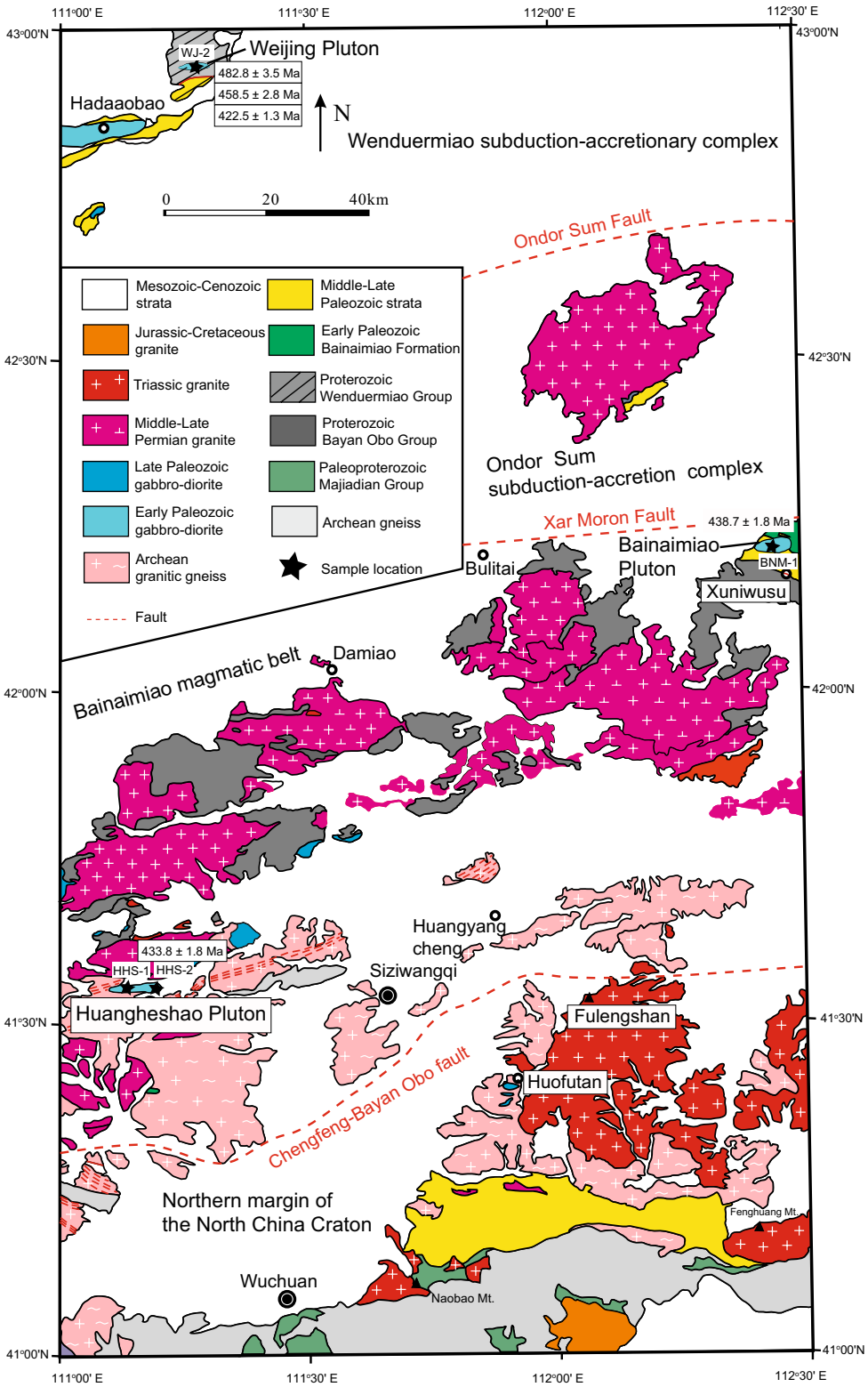

Fig. 2 Simplified geological map of the study area, modified from Liu et al. (2014) based on our own observations, showing sample localities

Stratigraphy and lithology

The study area covers three tectonic units of pre-Mesozoic from north to south, followed by the Wenduermiao subduction–accretionary complex, Bainaimiao island arc magmatic rock belt, and the northern margin of North China craton.

The Wenduermiao subduction–accretionary complex consists of Early Paleozoic Wenduermiao Group

metamorphic rocks, unconformably overlain by Late Paleozoic Carboniferous sedimentary rocks and Permian volcanic-sedimentary rocks. The Wenduermiao Group is subdivided into the Sangdahahuduge and Haerhada Formations. The Sangdahahuduge Formation consists of greenschists with quartzite lenses, and the Haerhada Formation consists of quartz schist, mica schist, greenschist, and quartzite with marble lenses. They are overlain by Carboniferous limestone, and Permian flysch, andesite, dolerite, sandstone, and limestone with a large number of brachiopod fossils. The pluton is composed of Cambrian–Ordovician granitoids, Permian diorite, quartz diorite, granodiorite (Zhou et al. 2009).

The oldest rocks exposed in the Bainaimiao magmatic belt are Middle Proterozoic metamorphic rocks of the Baiyunerbo Group, which consists of meta-sandstones and low P/T (pressure/temperature) metamorphic rocks, and Baiyinduxi Group consisting of quartz schist, felsic gneiss, amphibolites, and metamorphosed sandstone. Zhou et al. (1992) reported the Sm–Nd age of 1226 Ma for the Baiyinduxi Group of 1226 Ma, while Gu et al. (2012) suggested that the Baiyinduxi Group is Late Paleozoic in age according to detrital zircon U–Pb ages of the metamorphosed quartz sandstone. The Paleozoic strata are dominated by sedimentary sequences from the Ordovician Bainaimiao Formation to the Lower Permian Sanmianjing Formation. The Ordovician Bainaimiao Formation was interpreted as a Middle–Late Ordovician continental arc that consists mainly of metamorphosed basic rocks interbedded with sandstone, phyllite, and limestone (Liu et al. 2014). The Middle–Late Silurian Xuniwusu Formation is composed mainly of marine clastic rocks, limestone, tuff, and andesite, which unconformably underlies Bainaimiao Formation, and is overlain the Xibiehe Formation. The upper limestone contains abundant tabulate coral fossils of *Favosites*, *Heliolites*, *Mesofavosites*, *Halysites*, and *Catenipora* (Hu et al. 1987, 1990). The Xibiehe Formation is composed of shallow marine sandstone, limestone, slate, and reef, with a large number of Late Silurian coral fossils preserved in the limestone (Zhang et al. 2010). The strata of the Late Paleozoic mainly consist of sandstone, conglomerate, and bioclastic limestone. The plutons in these Formations are composed of Early Paleozoic granitic porphyry (Sm–Nd age of 440 ± 40 Ma) and variably deformed gneissic quartz diorite (zircon U–Pb ages of 459–454 and 445 Ma) (Tong et al. 2010; Li et al. 2012b). The Late Paleozoic syenogranite (zircon U–Pb age of 260 Ma) suggests that the pluton was related to the collision according to their geochemistry data (Zhang et al. 2009c; Liu et al. 2010a, b).

The exposed basement of the northern margin of North China craton is composed of highly metamorphosed Archean and Paleoproterozoic rocks, which includes major crustal building TTG (tonalite–trondhjemite–granodiorite) rocks, high K granite, and variably deformed diorite, which is characterized by major crustal growth and recycling tectonothermal events at ~2.5 Ga (Zhou et al. 2009; Zhai and Santosh 2011; Liu et al. 2014). The basement was unconformably covered by Mesoproterozoic–Neoproterozoic Bayan Obo Formation and Zhaertaishan Formation, Cambrian–Ordovician marine clastic and carbonate platformal sediments, Middle Carboniferous to Triassic fluvial and deltaic sediments, and Jurassic–Cretaceous younger volcanis and sedimentary rocks (Zhou et al. 2009; Zhang et al. 2014). The Late Paleozoic strata and intrusive rocks are well developed. The relationship between the North China craton and the Bainaimiao island arc belt is still highly controversial. Some researchers consider it as a continental arc in an active continental margin of the North China craton (Xiao et al. 2013; Liu et al. 2014), exotic terrains accreted to the northern margin of the North China craton (Li 1997), while others regarded the Bainaimiao island arc belt as a Japan-style island arc (Hu et al. 1990; Jia et al. 2003).

Sample petrology and analytical methods

Sample petrology

The Weijing granitoid sample WJ-2 (42°25.62′N, 111°16.40′E) is medium-grained gneissic quartz diorite and contains more biotite and less hornblende in comparison with the diorite (Figs. 3, 6). It consists of plagioclase (75–80 %), quartz (3–5 %), biotite (~15 %), and minor garnet (~5 %), together with accessory apatite, zircon, titanite, and magnetite. Plagioclase displays a complex zoned texture, which is characterized by hypidiomorphic–idiomorphic boards, polysynthetic twins, and simple double-crystal growth with sizes of 0.6–4.7 mm, and partly shows sericitization and epidotization.

The Bainaimiao granitoid sample BNM-1 (42°12.70′N, 112°25.67′E) is medium-grained diorite porphyrite (Figs. 3, 6). It has a porphyritic texture with approximately 35 % phenocrysts that are mainly composed of plagioclase (30 %) and minor melanocratic mineral (5 %). The plagioclase appears as hypidiomorphic boards, polysynthetic twins with sizes of 0.1–1.8 mm that partly show sericitization, while approximately 65 % stromas that are mainly composed of felsic (55 %) and accessory apatite, zircon, sericite, chlorite, and carbonate rock (~10 %).

The Huangheshao granitoid samples HHS1 and HHS2 (42°31.95′N, 111°10.62′E) are medium-coarse-grained syenite (Figs. 3, 6). They consist of K-feldspar (~85 %), plagioclase (~15 %), and minor melanocratic mineral, together with accessory apatite, zircon, and magnetite. The Huangheshao pluton is overlying unconformity Mesozoic strata. Yan et al. (1999) reported an Rb–Sr age of 203 Ma

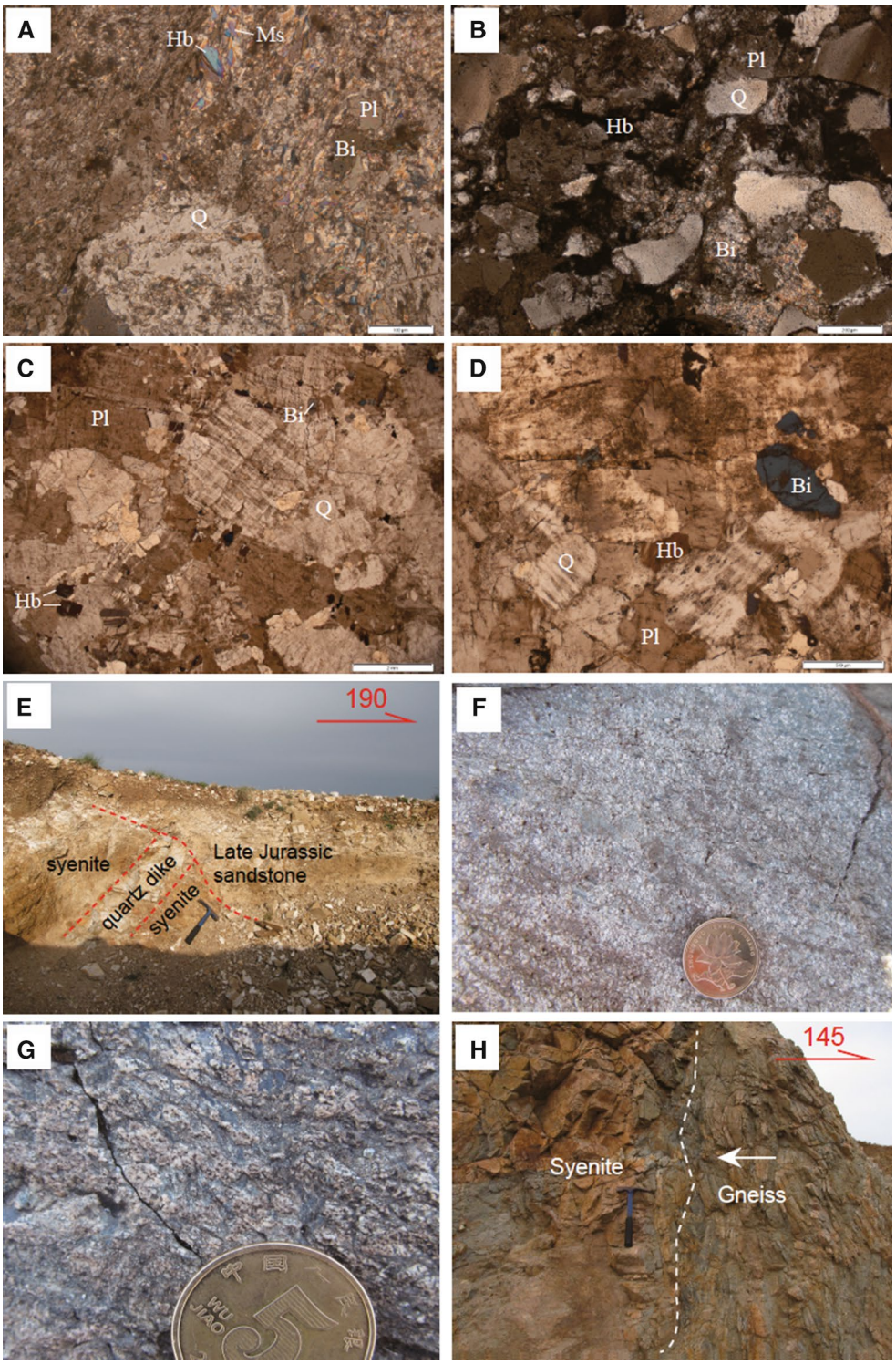

Fig. 3 Photographs of selected features of Siziwangqi granitoids. **a–d** Photomicrographs under plane polarized light showing the features of Weijing granitoid (WJ-2), Bainaimiao granitoid (BNM-1), and Huangheshao granitoids (HHS1 and HHS2), respectively. **e** The contact of the sandstone and the Huangheshao syenite. **f** The outcrop photograph showing the field occurrence of the Bainaimiao quartz diorite. **g** The outcrop photograph showing the field occurrence of the Weijing quartz diorite. **h** The outcrop photograph showing the Huangheshao syenite intruded into the gneiss. *Q* quartz, *PL* plagioclase, *kf* K-feldspar, *Bi* biotite, *Ms* muscovite, *Hb* hornblende

for the Huangheshao pluton, while we found that the pluton in turn was intruded by Permian medium syenite according to the field works (Fig. 3) (Liu et al. 2010a, b).

Analytical methods

Major oxides of samples were analyzed by X-ray fluorescence analysis (XRF; PHILIPS PW1480) using fused glass disks at the National Research Center for Geoanalysis, Chinese Academy of Geological Sciences (CAGS) in Beijing, China. The analytical uncertainties are less than 1 %, estimated from repeated analyses of two standards (andesite GSR-2 and basalt GSR-3). Loss on ignition was determined gravimetrically after heating the samples at 980 °C for 30 min. Uncertainties for most major oxides are <2 wt%, for MnO and P_2O_5 <5 wt%, and the totals are within 100 ± 1 wt%. Trace element analyses were determined by inductively coupled plasma mass spectrometry (ICP-MS) hosted in the National Research Center for Geoanalysis, Chinese Academy of Geological Sciences (CAGS) in Beijing, China. Precision for most elements was typically better than 5 % RSD (relative standard deviation), and the measured values for Zr, Hf, Nb, and Ta were within 10 % of the certified values. The detailed sample preparations, instrument operating conditions, and calibration procedures follow those established by Liang and Grégoire (2000). Two standards (granite GSR-1, basalt GSR-3) were used to monitor the analytical quality. The analytical errors vary from 3 to 7 % depending on the concentration of any given element. An internal standard was used for monitoring drift during analysis. The further details have been given by Gao et al. (2008). The detailed analytical results of this study are reported in Table 1.

Three titanomagnetite separates were concentrated using a combination of magnetic and heavy liquid techniques and further purified by handpicking at the mineral separation laboratory of the Bureau of Geology and Mineral Resources of Hebei Province at Langfang. Zircon grains were separated through conventional magnetic and density techniques to concentrate non-magnetic, heavy fractions. The grains were handpicked under a binocular microscope. Internal structures of the zircon grains were examined using transmitted electron, backscattered electron (BSE), and cathode luminescence (CL) prior to U–Pb isotopic analysis. The BSE imaging and CL imaging were taken by LEO1450VP scanning electron microscope with Mini CL detector at the Institute of Geology, Chinese Academy of Geological Sciences. Zircon analysis of these samples was performed on the Neptune multiple collector inductively coupled plasma mass spectrometer (Thermo Fisher Ltd.) with a 193-nm-FX Ar Excimer laser-ablation system (ESI Ltd.) at the Isotopic Laboratory, Tianjin Institute of Geology and Mineral Resources. NIST610 glass was used as an external standard to calculate U, Th, Pb concentrations of zircons, common Pb correction used the ^{208}Pb method (Andersen 2002), and TEMORA zircon (CITE STANDARD) was used as an external standard to normalize isotopic fractionation during the analysis. Uncertainties of individual analyses are reported with 1σ errors; weighted mean ages are reported at the 2σ confidence level. The age calculations and plotting of concordia diagrams were made using Isoplot (Ludwig 2003). The detailed analytical technique is described in Li et al. (2009). The detailed analytical results are reported in Table 2.

Analytical results

Major and trace elements

Four granitic samples (Fig. 6) were tested for major and trace element compositions. The loss on ignition (LOI) for most samples is about 1 wt%. According to the modal abundances (QAPF classification) (Fig. 6a), the Weijing granitoid rock is a quartz diorite and the Bainaimiao granitoid samples are diorite, whereas the Huangheshao sample falls into the syenite field.

The Weijing granitoid (WJ-2) is characterized by peraluminous (molar A/CNK = 1.92 and A/NK = 3.68) (Table 1). According to the K_2O versus SiO_2 diagram (Le Maitre 1984; Rickwood 1989), the sample plots in the calc-alkaline field (Fig. 6b), indicating a relatively oxydic magmatic evolution environment. The studied rock is characterized by low Sr (169 ppm) and Ba (376 ppm), high U (1.24 ppm) and La (16.7 ppm) (Table 1). The N-MORB normalized trace element concentrations display relative enrichment of large-ion lithophile elements (LILEs) and depletion of HFSEs, with negative Nb, P, K, Ti, and positive Pb, U, and La anomalies, consistent with a subduction-related setting (Fig. 6c). The chondrite-normalized REE patterns of the WJ-2 show an enriched LREE and flat HREE, with $(La/Yb)_N$ ratios of 5.60 [where N denotes normalized to chondrite values of Sun and Mcdonough (1989)] (Fig. 6d; Table 1); Eu and Yb exhibit well-defined negative trends ($\delta Eu = 0.44$).

The Bainaimiao granitoid (BNM-1) is characterized by peraluminous (molar A/CNK = 1.14 and A/NK = 1.89) (Table 1). According to the K_2O versus SiO_2 diagram (Le Maitre 1984; Rickwood 1989), this sample falls in the field of shoshonitic series (Fig. 6b), suggesting a relatively oxydic magmatic evolution environment. The sample is characterized by low Y (13.7 ppm), Ce (56.7 ppm), and HFSEs, and high Sr (682 ppm), Ba (898 ppm), and La (33.6 ppm) contents (Table 1). The N-MORB-normalized trace element concentrations display relative enrichment of large-ion lithophile elements (LILEs) and

Table 2 LA-ICP-MS results for zircons U–Pb ages of granitoid samples in this study

Analysis spot	Pb (ppm)	U (ppm)	Th/U	Isotopic ratios						Apparent ages (Ma)					
				$^{206}Pb/^{238}U$	1σ	$^{207}Pb/^{235}U$	1σ	$^{207}Pb/^{206}Pb$	1σ	$^{206}Pb/^{238}U$	1σ	$^{207}Pb/^{235}U$	1σ	$^{207}Pb/^{206}Pb$	1σ
HHS.2.1	87	1367	0.219	0.0694	0.0004	0.5318	0.0059	0.0556	0.0006	432	3	433	5	437	23
HHS.2.2	208	970	3.204	0.0921	0.0006	5.7447	0.0608	0.4522	0.0044	568	4	1938	21	4093	14
HHS.2.3	358	664	0.360	0.4954	0.0032	11.3723	0.1241	0.1665	0.0016	2594	17	2554	28	2523	16
HHS.2.4	18	272	0.191	0.0693	0.0004	0.5304	0.0192	0.0555	0.0020	432	3	432	16	434	81
HHS.2.5	16	233	0.422	0.0693	0.0005	0.5312	0.0267	0.0556	0.0028	432	3	433	22	438	111
HHS.2.6	20	303	0.145	0.0697	0.0005	0.5345	0.0195	0.0557	0.0019	434	3	435	16	439	77
HHS.2.7	11	192	1.103	0.0502	0.0004	0.3690	0.0154	0.0533	0.0021	316	2	319	13	341	90
HHS.2.8	99	1046	0.689	0.0739	0.0004	1.5313	0.0208	0.1503	0.0020	459	3	943	13	2350	23
HHS.2.9	14	324	0.559	0.0416	0.0003	0.3049	0.0087	0.0531	0.0015	263	2	270	8	333	63
HHS.2.10	35	524	0.223	0.0698	0.0004	0.5377	0.0091	0.0558	0.0009	435	3	437	7	446	36
HHS.2.11	31	456	0.259	0.0694	0.0005	0.5334	0.0447	0.0557	0.0049	433	3	434	36	442	195
HHS.2.12	10	150	0.183	0.0692	0.0005	0.5298	0.0371	0.0556	0.0038	431	3	432	30	435	154
HHS.2.13	402	731	0.679	0.4575	0.0027	10.6169	0.1067	0.1683	0.0016	2428	14	2490	25	2541	16
HHS.2.14	25	743	0.650	0.0314	0.0002	0.2191	0.0048	0.0506	0.0011	199	1	201	4	224	50
HHS.2.15	54	417	0.874	0.0723	0.0004	2.5054	0.0351	0.2515	0.0033	450	3	1274	18	3194	21
HHS.2.16	342	598	0.795	0.4740	0.0028	11.5514	0.1204	0.1768	0.0017	2501	15	2569	27	2623	16
HHS.2.17	241	481	0.317	0.4564	0.0028	10.6143	0.1115	0.1687	0.0016	2424	15	2490	26	2545	16
HHS.2.18	382	726	0.388	0.4672	0.0028	10.5885	0.1079	0.1644	0.0016	2471	15	2488	25	2501	16
HHS.2.19	204	347	0.850	0.4734	0.0029	10.9512	0.1113	0.1678	0.0016	2499	15	2519	26	2536	16
HHS.2.20	18	273	0.063	0.0703	0.0004	0.5419	0.1337	0.0559	0.0138	438	3	440	109	450	547
HHS.2.21	24	276	1.013	0.0698	0.0010	0.5365	0.1105	0.0557	0.0112	435	6	436	90	441	448
HHS.2.22	231	406	0.633	0.4818	0.0031	11.3519	0.1157	0.1709	0.0016	2535	16	2552	26	2566	16
HHS.2.23	31	375	0.934	0.0698	0.0006	0.5374	0.0361	0.0559	0.0037	435	4	437	29	447	148
HHS.2.24	12	150	0.669	0.0698	0.0005	0.5349	0.0198	0.0556	0.0020	435	3	435	16	435	81
BNM.1	10	116	0.638	0.0755	0.0008	0.6009	0.0243	0.0577	0.0022	469	5	478	19	519	83
BNM.2	19	230	0.973	0.0712	0.0007	0.5627	0.0145	0.0573	0.0014	444	4	453	12	503	54
BNM.3	22	224	1.090	0.0767	0.0008	0.8423	0.0215	0.0796	0.0018	476	5	620	16	1188	46
BNM.4	16	208	0.548	0.0708	0.0007	0.5657	0.0153	0.0580	0.0015	441	4	455	12	529	57
BNM.5	17	220	0.676	0.0707	0.0007	0.5591	0.0172	0.0574	0.0017	440	4	451	14	505	66
BNM.6	16	201	0.691	0.0705	0.0007	0.5611	0.0154	0.0577	0.0015	439	4	452	12	520	58
BNM.7	12	161	0.566	0.0713	0.0007	0.5513	0.0193	0.0561	0.0019	444	5	446	16	456	74
BNM.8	13	164	0.768	0.0702	0.0007	0.5519	0.0173	0.0570	0.0017	437	4	446	14	492	66
BNM.9	17	167	0.837	0.0772	0.0008	1.1386	0.0332	0.1069	0.0028	480	5	772	23	1747	47
BNM.10	23	284	1.082	0.0706	0.0007	0.5700	0.0130	0.0585	0.0013	440	4	458	10	550	48
BNM.11	11	143	0.695	0.0718	0.0007	0.5581	0.0225	0.0564	0.0022	447	5	450	18	466	85

Table 2 continued

Analysis spot	Pb (ppm)	U (ppm)	Th/U	Isotopic ratios						Apparent ages (Ma)					
				$^{206}Pb/^{238}U$	1σ	$^{207}Pb/^{235}U$	1σ	$^{207}Pb/^{206}Pb$	1σ	$^{206}Pb/^{238}U$	1σ	$^{207}Pb/^{235}U$	1σ	$^{207}Pb/^{206}Pb$	1σ
BNM.12	23	291	0.814	0.0704	0.0007	0.5439	0.0133	0.0561	0.0013	438	4	441	11	455	52
BNM.13	10	128	0.856	0.0698	0.0007	0.5415	0.0205	0.0563	0.0021	435	4	439	17	464	82
BNM.14	9	127	0.540	0.0698	0.0008	0.5354	0.0334	0.0556	0.0034	435	5	435	27	437	135
BNM.15	11	137	0.951	0.0710	0.0007	0.5635	0.0225	0.0576	0.0022	442	5	454	18	514	82
BNM.16	23	277	1.115	0.0690	0.0007	0.5587	0.0123	0.0587	0.0012	430	4	451	10	556	46
BNM.17	10	131	0.855	0.0698	0.0009	0.5493	0.0698	0.0570	0.0072	435	6	445	57	493	279
BNM.18	8	103	0.646	0.0706	0.0007	0.5432	0.0272	0.0558	0.0027	440	5	441	22	445	109
BNM.19	60	670	1.473	0.0712	0.0007	0.5599	0.0086	0.0570	0.0008	444	4	451	7	491	31
BNM.20	37	457	1.080	0.0699	0.0007	0.5386	0.0169	0.0559	0.0017	435	4	437	14	449	68
BNM.21	33	397	1.093	0.0704	0.0007	0.5479	0.0145	0.0565	0.0015	438	4	444	12	471	57
BNM.22	21	258	0.910	0.0702	0.0007	0.5460	0.0157	0.0564	0.0016	437	4	442	13	470	62
BNM.23	12	151	0.719	0.0699	0.0007	0.5465	0.0314	0.0567	0.0032	435	5	443	25	481	124
BNM.24	25	302	0.814	0.0699	0.0007	0.5453	0.0145	0.0565	0.0014	436	4	442	12	474	56
BNM.25	26	334	0.615	0.0704	0.0007	0.5423	0.0106	0.0559	0.0010	438	4	440	9	448	41
BNM.26	26	309	1.006	0.0705	0.0007	0.5508	0.0119	0.0567	0.0011	439	4	446	10	478	45
BNM.27	13	175	0.672	0.0702	0.0007	0.5460	0.0197	0.0564	0.0020	437	4	442	16	469	77
WJ2.1	33	419	0.520	0.0739	0.0004	0.5727	0.0122	0.0562	0.0012	460	2	460	10	460	46
WJ2.2	39	498	0.281	0.0782	0.0004	0.6147	0.0098	0.0570	0.0009	485	3	487	8	493	34
WJ2.3	23	323	0.185	0.0734	0.0004	0.5681	0.0090	0.0561	0.0009	457	2	457	7	457	35
WJ2.4	28	394	0.182	0.0738	0.0004	0.5746	0.0087	0.0565	0.0008	459	2	461	7	472	33
WJ2.5	15	224	0.307	0.0678	0.0004	0.5189	0.0128	0.0555	0.0014	423	2	424	10	433	55
WJ2.6	9	140	0.249	0.0676	0.0005	0.5189	0.0430	0.0557	0.0046	422	3	424	35	439	183
WJ2.7	12	181	0.326	0.0678	0.0004	0.5192	0.0148	0.0556	0.0016	423	2	425	12	435	63
WJ2.8	7	107	0.349	0.0677	0.0007	0.5172	0.0408	0.0554	0.0042	422	4	423	33	429	171
WJ2.9	19	276	0.365	0.0678	0.0004	0.5195	0.0134	0.0556	0.0014	423	2	425	11	436	57
WJ2.10	12	177	0.327	0.0677	0.0004	0.5180	0.0205	0.0555	0.0022	422	2	424	17	433	87
WJ2.11	26	333	0.371	0.0776	0.0004	0.6110	0.0098	0.0571	0.0009	482	3	484	8	495	35
WJ2.12	34	418	0.538	0.0776	0.0006	0.6089	0.0227	0.0569	0.0021	482	3	483	18	488	81
WJ2.13	10	157	0.259	0.0678	0.0004	0.5171	0.0236	0.0553	0.0025	423	3	423	19	424	101
WJ2.14	12	179	0.331	0.0678	0.0004	0.5172	0.0225	0.0553	0.0024	423	3	423	18	425	96
WJ2.15	10	145	0.314	0.0676	0.0004	0.5166	0.0335	0.0554	0.0036	422	3	423	27	428	144
WJ2.16	12	177	0.362	0.0679	0.0005	0.5201	0.0512	0.0556	0.0058	423	3	425	42	436	230
WJ2.17	10	150	0.317	0.0678	0.0004	0.5165	0.0172	0.0553	0.0018	423	2	423	14	423	73
WJ2.18	10	156	0.354	0.0677	0.0004	0.5186	0.0163	0.0556	0.0017	422	2	424	13	436	69
WJ2.19	20	252	0.394	0.0783	0.0004	0.6140	0.0122	0.0569	0.0011	486	3	486	10	487	43

Table 2 continued

Analysis spot	Pb (ppm)	U (ppm)	Th/U	Isotopic ratios						Apparent ages (Ma)					
				$^{206}Pb/^{238}U$	1σ	$^{207}Pb/^{235}U$	1σ	$^{207}Pb/^{206}Pb$	1σ	$^{206}Pb/^{238}U$	1σ	$^{207}Pb/^{235}U$	1σ	$^{207}Pb/^{206}Pb$	1σ
WJ2.20	18	244	0.063	0.0781	0.0005	0.6134	0.0104	0.0569	0.0009	485	3	486	8	489	36
WJ2.21	13	194	0.348	0.0678	0.0004	0.5192	0.0150	0.0555	0.0016	423	2	425	12	433	63
WJ2.22	10	146	0.269	0.0676	0.0005	0.5186	0.0376	0.0556	0.0039	422	3	424	31	436	156
WJ2.23	15	220	0.361	0.0677	0.0004	0.5172	0.0129	0.0554	0.0014	422	2	423	11	428	55
WJ2.24	175	854	0.111	0.2111	0.0012	2.6292	0.0257	0.0903	0.0008	1235	7	1309	13	1433	18
WJ2.25	56	722	0.377	0.0768	0.0004	0.6028	0.0065	0.0569	0.0006	477	3	479	5	488	23

depletion of HFSEs, with negative Nb, Pr, Ti, P, K and positive Pb, and Sr anomalies, consistent with a subduction-related setting (Fig. 6c). The chondrite-normalized REE patterns of the BNM-1 show an enriched LREE and flat HREE, with $(La/Yb)_N$ ratios of 15.45 (Fig. 6d; Table 1); Eu and Yb exhibit well-defined negative trends ($\delta Eu = 0.32$).

The Huangheshao granitoids (HHS1 and HHS2) are characterized by peraluminous (molar A/CNK = 1.005–1.013 and A/NK = 1.021–1.028) (Table 1). According to the K_2O versus SiO_2 diagram (Le Maitre1984; Rickwood 1989), both samples fall in calc-alkaline field (Fig. 6b), which reflects a relatively oxydic magmatic evolution environment. Both the studied samples are characterized by low Ta (0.12–0.13 ppm), Dy (0.18–0.26 ppm), and Ce (8.04–8.19 ppm), and high Pb (7.68–14.2 ppm), Sr (99.9–130 ppm), and La (3.85–3.93 ppm) contents (Table 1). Their N-MORB-normalized trace element concentrations display relative enrichment of large-ion lithophile elements (LILEs) and depletion of HFSEs, with negative P, Ta, Ti, and positive Pb, and Sr anomalies (Fig. 6c). The chondrite-normalized REE patterns of the HHS1 and HHS2 show an enriched LREE and flat HREE, with $(La/Yb)_N$ ratios of 21.24–23.49 (Fig. 6d; Table 1); Eu and Yb exhibit well-defined negative trends ($\delta Eu = 0.32–0.33$).

Zircon U–Pb geochronology

Weijing granitoid

Zircons from Weijing granitoid are mostly elongated columns, with a small portion of short columns. Grains are between 100 and 260 μm long. Most zircons are colorless, with a few that are yellow–brown in color. The CL images indicate that most zircons have clear growth zoning (Fig. 4). Some of them display sector zoning, strip zoning, homogeneous in oval shape or clear core–mantle structure (Fig. 4). The U content of the 20 spots is between 68.3 ppm and 736.2 ppm with a U/Th ratio of 0.43–0.98 (average 0.64). Therefore, the analyzed zircons are of magmatic origin (e.g., Pearce et al. 1984; Le Maitre 1984). In the $^{206}Pb/^{238}U$–$^{207}Pb/^{235}U$ concordia diagram (Fig. 5a), zircon populations are complex in this sample. The grain from one zircon is characterized by a Mesoproterozoic upper intercept of 1309 Ma (point WJ-2-24) (Fig. 5a). Other grains are prismatic with oscillatory zoning (Fig. 4) and form three populations (Fig. 5a): 482.8 ± 3.5 Ma (MSWD = 1.5), 458.5 ± 2.8 Ma (MSWD = 0.39), and 422.5 ± 1.3 Ma (MSWD = 0.026) (Fig. 5a). These analyzed points for the 25 zircons are located on the concordia and nearby, representing the crystallization ages. We thus suggest the younger 422.5 ± 1.3 Ma age of pluton crystallization.

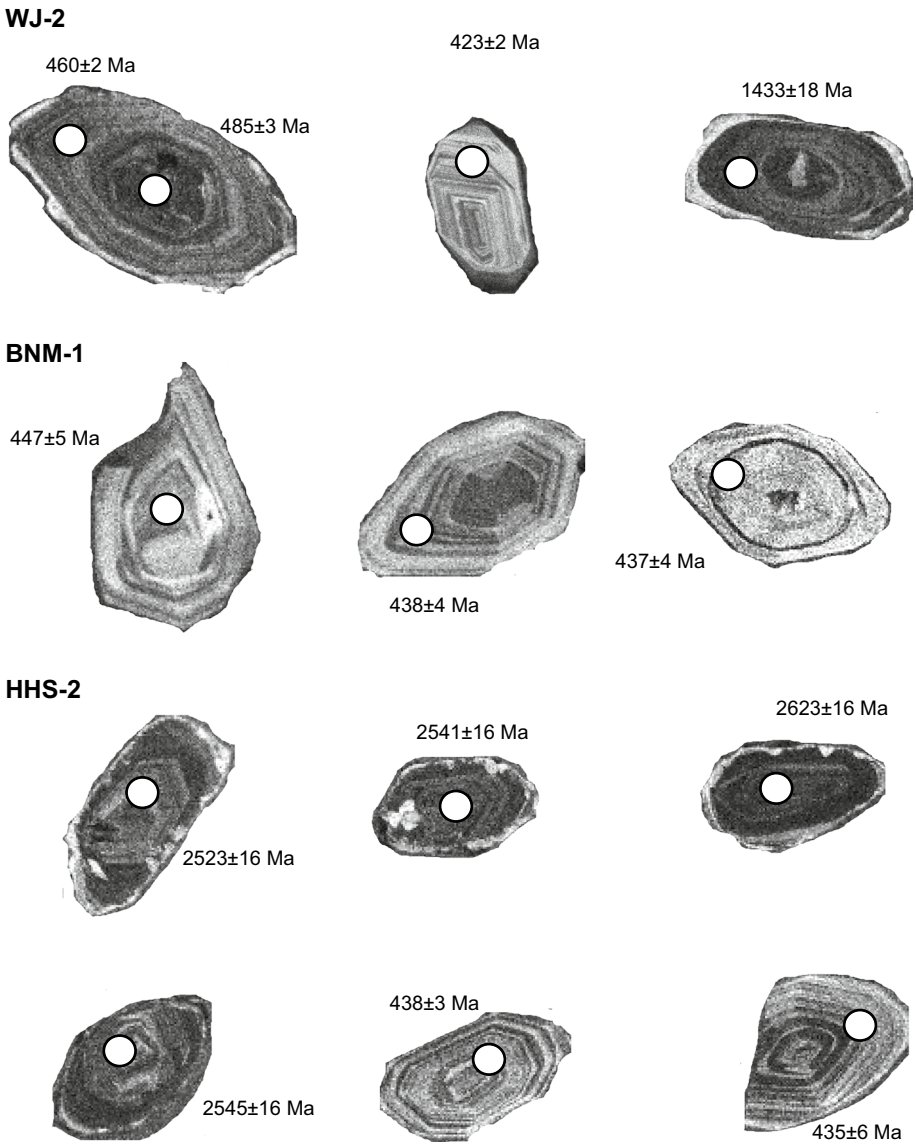

Fig. 4 Cathodoluminescence (CL) images of zircons from representative samples. *Black circles* with white outlines are analyzed spots. The *numerals* are ages in Ma

Older ages of 482.8 ± 3.5 and 458.5 ± 2.8 Ma are interpreted to represent the ages of inherited zircon.

Bainaimiao granitoid

Most zircons appear as elongated columns, with small portions of short columns. The size is between 100 μm and 230 μm. The zircons are mostly colorless, with few yellowish brown ones. The CL images indicate that most zircons have clear growth zoning (Fig. 4). The U/Th ratios of the 27 zircons are greater than 0.1, with U content of 103–670 ppm. Twenty-seven analyses define a single concordant population on a $^{206}Pb/^{238}U$–$^{207}Pb/^{235}U$ concordia diagram (Fig. 5b) with a weighted average $^{206}Pb/^{238}U$ age of 438.7 ± 1.8 Ma (MSWD = 0.70), which we interpret to represent the crystallization age (Fig. 5b).

Huangheshao granitoid

Zircons are mostly elongated columns, with a small portion of short columns. The size is between 100 and 250 μm. They are mostly colorless, with few yellowish brown. The CL images indicate that most zircons have clear growth zoning (Fig. 4). Some of them display sector zoning, strip zoning, homogeneous in oval shape or clear core-mantle structure (Fig. 4). The U/Th ratios of the 24 zircons are greater than 0.1 with U content of 150–1046 ppm. In the $^{206}Pb/^{238}U$–$^{207}Pb/^{235}U$ concordia diagram (Fig. 5c), zircon populations are complex in this sample. They yield an Archean intercept of age of ~2500 Ma, and Early Paleozoic concordant age of 433.8 ± 1.8 Ma (MSWD = 0.89) representing the crystallization age (Fig. 5c). The concordia age of the remaining one zircon is 263 ± 3 Ma (point HHS-1-9), and it should be the captured late magmatic zircon. We

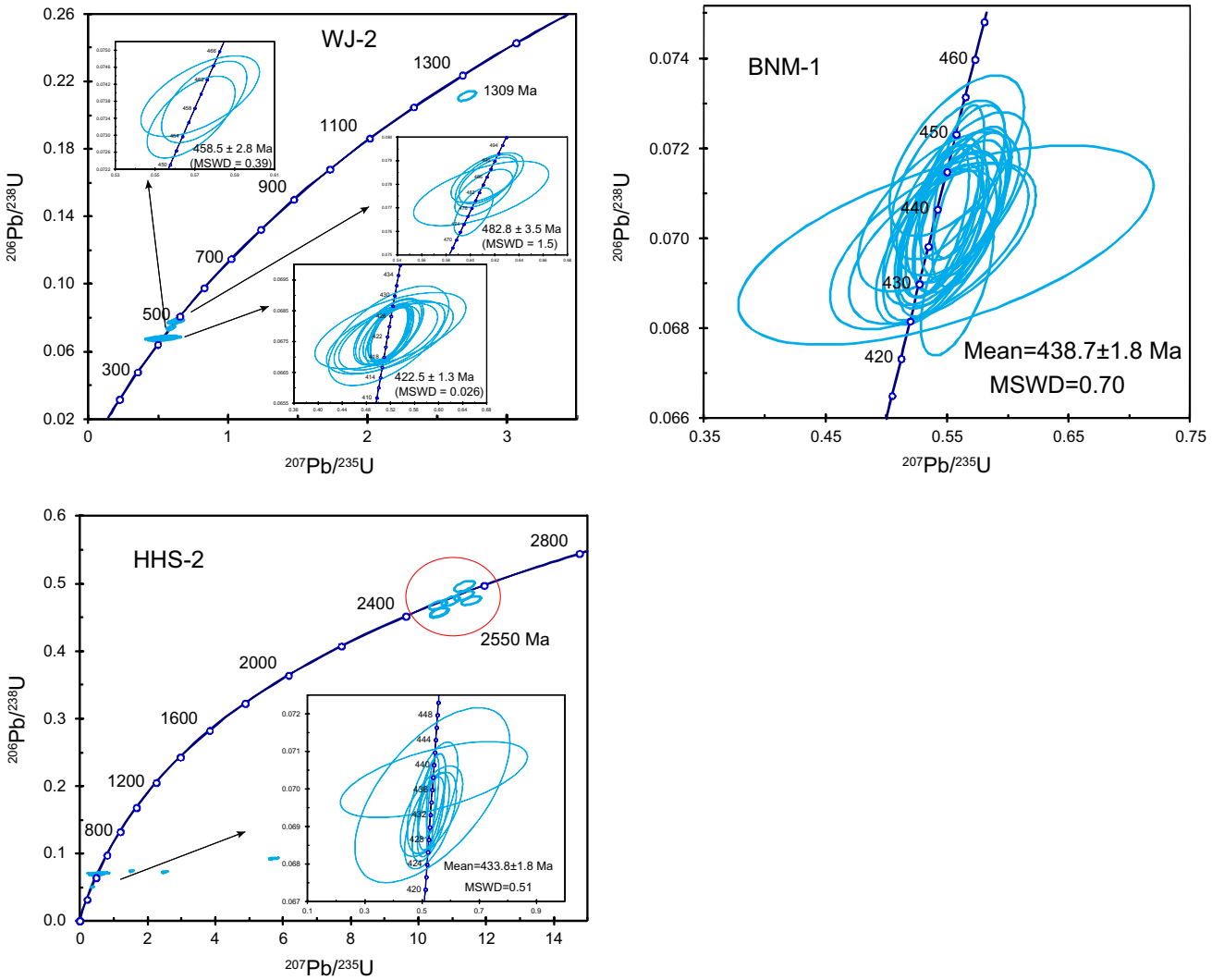

Fig. 5 Zircon $^{207}Pb/^{235}U$–$^{206}Pb/^{238}U$ concordia diagrams of Early Paleozoic granitoid samples from this study

note that the 263 ± 3 Ma zircon age is similar to the Wuerta pluton (Liu et al. 2015) with the geochemistry characteristic of partial melting of thickened crust which intrudes into the Solonker ophiolite (Jian et al. 2010; Liu et al. 2015), so we suggest that the tectonic events related to the continent–continent collision in this region.

Discussion

Age and petrogenesis

The Wenduermiao subduction–accretionary complex consists of the Wenduermiao Group, Tulinkai ophiolite, and Early Paleozoic pluton. Many controversies have still existed about the formation age and the nature of the Wenduermiao Group (i.e., Xu et al. 1994; Xiao et al. 2003; Jian et al. 2008). The Wenduermiao Group might be consists of rocks of the different periods and different petrogenesis, which, respectively, belong to intra-oceanic arc, forearc accretionary wedge, oceanic crust (Liu et al. 2003; De Jong et al. 2006; Li et al. 2012a). We suggest that the formation age of the Wenduermiao Group is Cambrian–Middle Silurian based on the following reasons: (1) the greenschist Rb–Sr age, K–Ar age, and glaucophane ^{40}Ar–^{39}Ar age of the Lower Wenduermiao Group (Sangdahahuduge Formation) are 435 ± 61 Ma, 473–436 Ma, and 445.6 ± 15 Ma, respectively (Tang et al. 1983; Tang 1992). In additional, the zircon U–Pb ages of the adakitic dacite and meta-andesite are 458 Ma and 470 ± 2 Ma (Tang and Yan 1993; Liu et al. 2003); (2) the quartz schist Rb–Sr age of the Upper Wenduermiao Group (Haerhada Formation) is 509 ± 40 Ma, and De Jong et al. (2006) obtained muscovite ^{40}Ar–^{39}Ar ages of the quartz mylonites of 453.2 ± 1.8 Ma and 449 ± 1.8 Ma. Moreover,

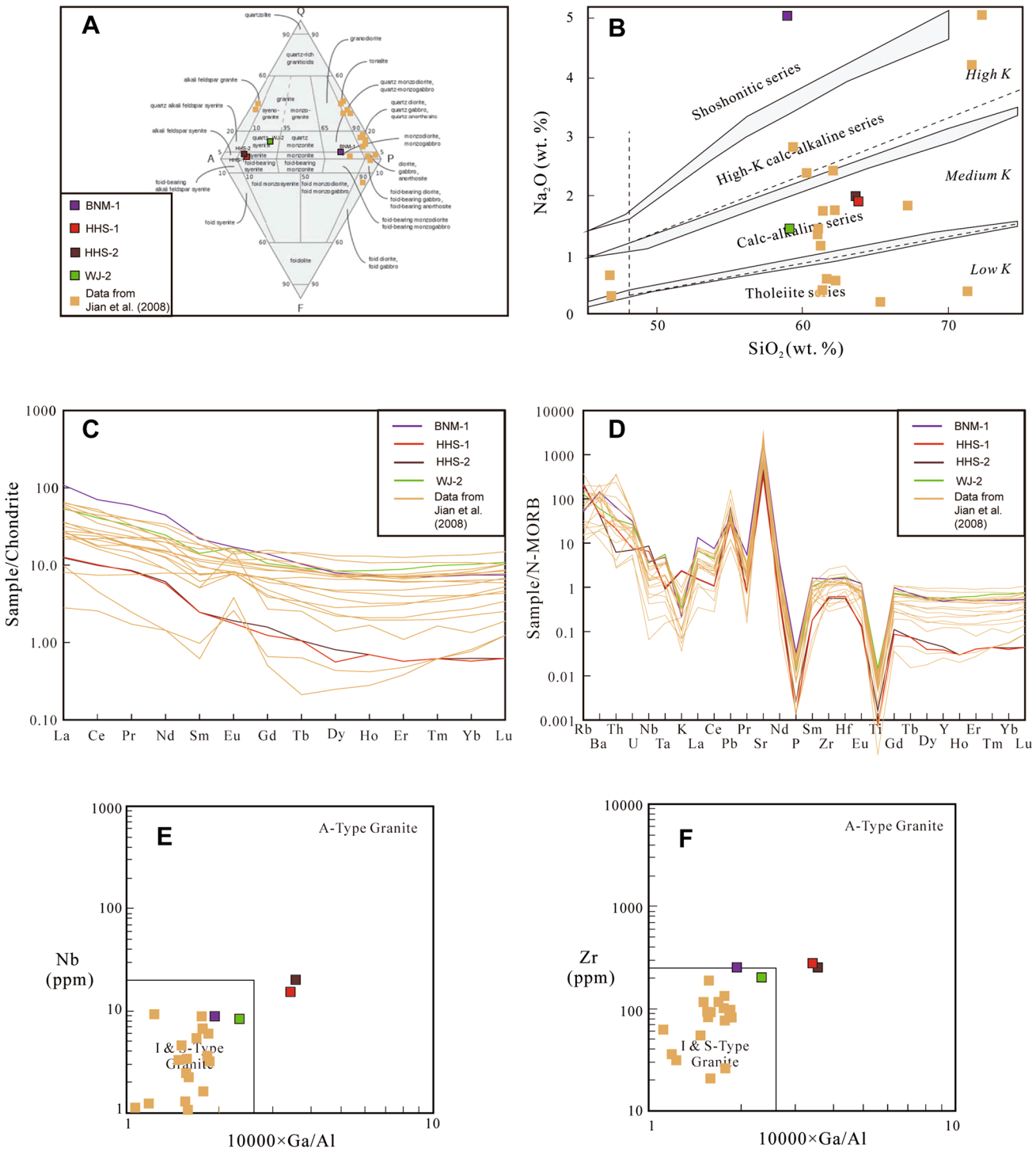

Fig. 6 Geochemistry diagrams for the granites from the study area. Data from Jian et al. (2008) and this study. **a** Petrographic classification based on the QAPF diagram (Streckeisen 1973) of granitoids from the study area. **b** K_2O versus SiO_2 diagram for intrusive rocks. Normalization values are from Le Maitre (1989) and Rickwood (1989). **c** Chondrite-normalized REE diagram for the granitoid samples from the different area of the study area. Normalization values are from Boynton (1984). **d** N-MORB-normalized spider diagram for the granitoid samples. Normalization values are from Sun and McDonough (1989). **e** (10,000 Ga/Al) versus Nb diagram for A-type granitoids (Whalen et al. 1987), and **f** (10,000 Ga/Zr) versus Zr diagram for A-type granitoids (Whalen et al. 1987)

the detrital zircon ages of Haerhada Formation show that the main peak of the zircon ages is 480–445 Ma, the youngest age peak is 438–424 Ma, and the weighted mean age is 431 ± 4.3 Ma (Li et al. 2012a). Liu et al. (2003) suggested that at least two oceanic crust subduction events occurred according to the zircon U–Pb ages of the adakitic quartz diorite, monzonitic granite and plagioclasite from the Tulinkai ophiolite are 467 ± 13 Ma, 451 ± 7 Ma, and 429 ± 7 Ma, respectively. Jian et al. (2008) suggested that the formation age of the suprasubduction zone (SSZ) Tunlinkai ophiolite is 497–477 Ma; the zircon U–Pb ages of the plagioclase granite and gabbro are 490.1 ± 7.1 Ma and 479 ± 2.4 Ma, respectively. Recently, Zhou et al. (2009) reported that the zircon U–Pb age of the Hadaaobao diorite is 508 Ma, which suggests that the subduction event started before ~508 Ma. In this study, we propose 422.5 ± 1.3 Ma as the crystallization age of the Weijing quartz diorite, which should be the minimum age of the Wenduermiao Group sedimentary sequence. Based on our geochemistry data, we suggest that the quartz diorite is the product of the subduction (Fig. 6). We also obtain two other ages of 482.8 ± 3.5 and 458.5 ± 2.8 Ma, which suggest the zircon information from the Wenduermiao Group sedimentary sequence because they intruded into the Wenduermiao Group strata. In summary, the age of the formation of the Wenduermiao subduction–accretionary complex is suggested to be the Middle Cambrian–Late Silurian (509–421 Ma), which consists of the age of oceanic crust, different stages of arc magmatic rocks, and forearc sedimentary.

Bainaimiao island arc belt consists of the meta-volcani-sedimentary sequence and the Early Paleozoic pluton. Some researchers suggested that the Bainaimiao Formation shows the characteristic of island arc rather than the continental margin rift ogenesis, which is the production of Early Paleozoic oceanic subduction (Hu et al. 1990; Shao 1991; Tang 1992; Zhou et al. 1992; Nie et al. 1995; Zhang and Wu 1999a, b), but the age of its formation is controversial. Zhang et al. (2013) reported that the zircon U–Pb ages of the biotite granulite and greenschist are 499.4 ± 1.8 and 478.1 ± 1.6 Ma, respectively. They also suggested that the Bainaimiao volcanics were formed during three episodes of 474 ± 7, 453 ± 7, and 436 ± 9 Ma; broadly synchronous, the low P/T metamorphic complex was affected by two distinct anatectic events at 462 ± 11 and 437 ± 5 Ma. Liu et al. (2014) proposed that the age of Bainaimiao meta-volcanic rock was 449 ± 3 Ma. Thus, we suggest that the formation period of the Bainaimiao meta-volcani-sedimentary sequence is of the Late Cambrian–Late Ordovician. There is a large of numbers Early Paleozoic intrusions in the Bainaimiao island arc belt. The Sm–Nd age of the granite porphyry is 440 ± 40 Ma (Nie et al. 1995), the zircon U–Pb ages of the granodiorite and quartz diorite are 445 and 459–454 Ma (Li et al. 2012b; Tong et al. 2010), and the zircon U–Pb age of dioritic intrusion is 438 ± 2 Ma (Zhang et al. 2013). In this study, the emplacement of a slightly gneissic quartz diorite pluton into the meta-volcanic rocks at 438.7 ± 1.8 Ma reflects the minimum age of the formation of the meta-volcanic, which is the last period of the arc magmatic event in the study area. In conclusion, we suggest that the tectonic nature of the Bainaimiao island arc belt is continental marginal arc, and the time of activity could be in the Late Cambrian–Early Silurian (501–437 Ma).

We suggested the existence of the back-arc basin between the Bainaimiao island arc belt and the North China craton according to our field observation and the zircon U–Pb ages. The Middle–Upper Silurian Xuniwusu Formation is the typical sedimentary sequence of the back-arc basin, related to the subduction. The Xuniwusu Formation is composed of coarse flysch in the lower part and sandy-silty flysch in the upper part. The exposed rocks of the lower part of Xuniwusu Formation are quartz sandstone, stuff within the slate, and phyllite, which unconformity overlie the underlying andesitic island arc pyroclastic-sedimentary rocks of Ordovician–Early Silurian period (Bainaimiao Formation). The Middle–Upper strata are thick limestone that covered unconformably the overlying by marine molasses sediments of terminal Late Silurian period (Xibiehe Formation). The flysch in the Bainaimiao area exhibits a rather complete rhythmical texture and a bedding structure with a great variety of flysch casts, which are typical turbidity current sediments (Hu et al. 1987, 1990; *BGMRN, 1991*). We found some coral fossils, including *Favosites*, *Heliolites*, *Mesofavosites*, *Halysites*, and *Catenipora* in the limestone. Additionally, we obtain a U–Pb zircon age of the Huangheshao syenites of 433.8 ± 1.8 Ma. This is the first time that a magmatic event of the back-arc basin is documented, indicating that the back-arc basin must have opened prior to Early Silurian lasted until the Late Silurian and have a formation age that is slightly later than the Bainaimiao island arc.

Nature of the basement

In this study, we obtain the inherited zircon U–Pb ages from the Weijing diorite at 1433 ± 18 Ma, while other researchers found the 1.5 Ga–1.2 Ga age from the meta-sandstones of the Wenduermiao Group (Li et al. 2012a; Zhou et al., unpublished). But there is no report of older ages. Zhang et al. (2009a) suggested the inherited zircon U–Pb ages from the vein into the Xuniwusu Formation at 1.9 Ga–1.26 Ga. Liu et al. (2014) reported some different phases inherited zircon U–Pb ages of the Bainaimiao meta-volcanic rocks at 1393 ± 19, 1746 ± 17 Ma, and 2286 ± 15. We also get the inherited zircon U–Pb ages from the Huangheshao syenites of 2548 Ma. Obviously, there are different basements between the Wenduermiao subduction–accretionary complex and the Bainaimiao island arc belt. The Wenduermiao subduction–accretionary complex could belong to the early oceanic crust and the XilinHot microcontinental block, while the basement of the Bainaimiao island arc belt should be the North China

craton. Also, Zhang et al. (2014) suggested that the Bainaimiao island arc belt is an ensialic island arc characterized by very different tectonic history and basement compositions than the northern North China craton according to their new research results. We suggest the existence of the Wenduermiao Ocean between the Wenduermiao subduction–accretionary complex and the Bainaimiao island arc belt in Early Paleozoic.

Tectonic evolution

The tectonic evolution of NE China includes the Paleozoic to Early Mesozoic subduction and the closure of the Paleo-Asia oceans (e.g., Sengör and Natal'in 1996; Wu et al. 2002, 2014, 2015), followed immediately by the initiation of westward subduction of the Pacific plate below eastern Asia (e.g., Şengör and Natal'in 1996; Wu et al. 2002). The Early Paleozoic zone of central Inner Mongolia was constructed over the Neoproterozoic to Early Mesozoic orogen variably named as the Central Asian Fold Belt (Zonenshain et al. 1990), Central Asian Accretionary Orogen (Sengör and Natal'in 1996), Central Asian Orogenic Belt (Jahn et al. 2004; Kröner et al. 2014), or Central Asian Orogenic System (Briggs et al. 2009) as the orogen is neither linear nor involving purely accretionary process. Island arcs and microcontinents may have played important roles in the formation of the huge CAOB (Zhang et al. 2009b, 2014). Paleozoic island arcs with buried Precambrian microcontinents are probably very common within the CAOB. Some researchers supported the evolutionary model of CAOB that involved subduction–collision–accretion processes of multiple island arcs and microcontinents (e.g., Xiao et al. 2003; Windley et al. 2007; Zhang et al. 2014). Specifically, the northern margin of the North China craton remained as a passive continental margin during the Early Paleozoic and transformed to an active continental margin from the Late Carboniferous (Zhang et al. 2009c, 2014). Also, the initiation of the Bainaimiao island arc in the southeastern CAOB occurred during the Early Cambrian period, and the arc was formed by northward subduction of the Paleo-Asian oceanic plate beneath a Proterozoic microcontinent with tectonic affinity to the South China craton (BGMRIM 1991; Zhang et al. 2014). The final accretion of the Bainaimiao island arc to the North China craton by arc–continent collision during the Late Silurian, the arc–continent collision was accompanied by metamorphism and deformation of the Early Paleozoic sedimentary, magmatic rocks and deposition of the Late Silurian–earliest Devonian continental molasses of the Xibiehe Formation (BGMRIM 1991; Zhang et al. 2009a, 2014; Liu et al. 2014). Magmatic rocks from the Bainaimiao island arc belt exhibit mainly 479–472, 453–438, and 427–411 Ma, and minor 518–499 Ma (Zhang et al. 2014). The latest magmatism as represented by an Early Devonian underformed pegmatite dike emplaced into the Ordovician to Silurian metamorphic rocks in the Bainaimiao area with a zircon U–Pb age of 411 Ma (Zhang et al. 2013), which suggests termination of the Bainaimiao island arc prior to the Early Devonian (Li et al. 2014; Zhang et al. 2014; Liu et al. 2014). We have undertaken major and trace element analyses of granitoid rocks in the central Inner Mongolia, as well as U–Pb dating analysis of their zircons, in order to determine the petrogenesis and tectonic setting of the granitoids and provide significant insights into the Early Paleozoic tectonic evolution in the southeastern segment of the long-lived Central Asian Orogenic Belt. The lithological association, mineral assemblage (Fig. 3), and geochemical compositions (Table 1) of the Early Paleozoic magmatic rocks in the Bainaimiao island arc belt indicate that they are subduction-related I-type granitoids formed in arc tectonic setting (Barbarin 1999), specifically the depletion in high field strength trace elements on primitive mantle-normalized diagrams (Fig. 6), which is further supported by the results of Zhang et al. (2014). Based on our new zircon ages and geochemical data, we conclude that the formation age of the Wenduermiao subduction–accretionary complex is Middle Cambrian–Late Silurian (509–421 Ma), which consists of oceanic crust, many stages arc magmatic rocks, and forearc sedimentary. The tectonic setting of the Bainaimiao island arc belt is a continental marginal arc that was active in the Late Cambrian–Early Silurian (501–437 Ma). This is the first time report about the magmatic event of the back-arc basin likely reflect the back-arc basin must opened prior to Early Silurian and till Late Silurian to close, and the formation age is slightly later than Bainaimiao island arc. The Wenduermiao subduction–accretionary complex could be the early oceanic crust and the XilinHot microcontinental block, while the basement of the Bainaimiao island arc belt should be the North China craton. In addition, we suggest that the Wenduermiao Ocean between the Wenduermiao subduction–accretionary complex and the Bainaimiao island arc belt existed in Early Paleozoic. As above, we suggest that the study area should be divided into five phases in Early Paleozoic according to petrology, chronology, geochemistry, and our field observation, with a possible model to explain these five phases are proposed below. We note that it is challenging to test the model as it requires careful reconstruction of the position and history of subducted Paleo-Asian oceanic slabs with highly interpretative tomographic images.

(A) Early Cambrian–Middle Cambrian (>510 Ma): The Zhaertaishan-Bayan Obo of the northern margin of the North China craton is a stable continental margin. The Wenduermiao Ocean already existed in this period with the XilinHot microcontinental in the northern part (Fig. 7a).

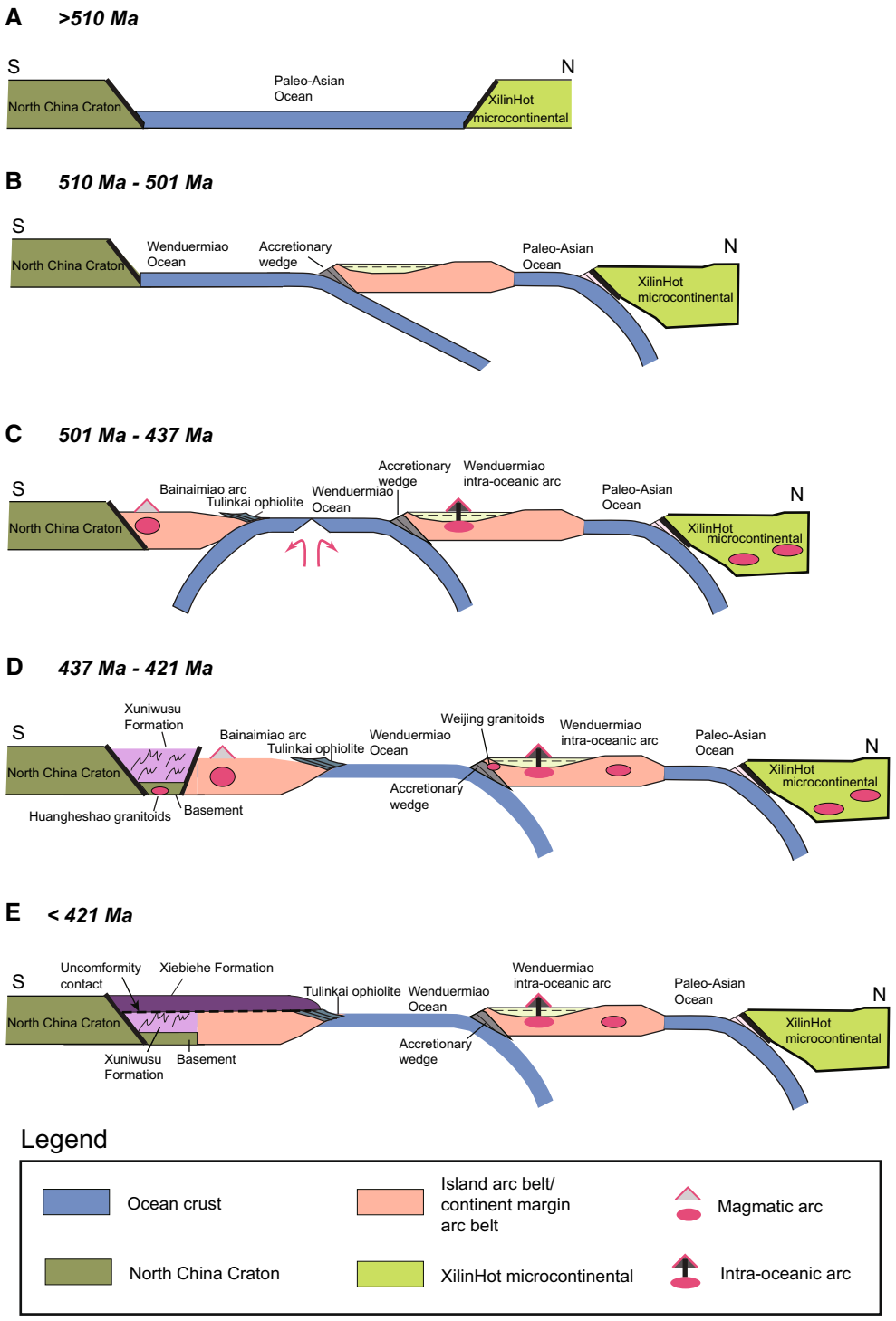

Fig. 7 A suggested petrogenetic–tectonic model for the southeastern Central Asian Orogenic Belt during the Early Paleozoic

(B) Middle Cambrian–Late Cambrian (510–501 Ma): The northward subduction of the Wenduermiao Ocean started in the late of the Middle Cambrian. The early period arc magmatic rocks formed on the basement of the oceanic crust; meanwhile, the formation of the Wenduermiao subduction–accretionary complex was starting (Fig. 7b).

(C) Late Cambrian–Middle Silurian (501–437 Ma): The North China craton changed from passive continental margin to active continental margin in the end of the Late Cambrian. The Wenduermiao Oceanic plate subducted southward beneath the North China craton and entered the bilateral subduction phase. At the same time,

the Wenduermiao intra-oceanic arc, arc magmatic rocks, and two arc magmatic belt of the Bainaimiao island arc were formed during the subduction. Additionally, the ophiolite and accretionary complex developed at the front of the subduction zone (Fig. 7c).

(D) Middle Silurian–Early Silurian (437–421 Ma): The successive northward subduction of the Wenduermiao Oceanic plate still continue, while the southward subduction stopped during the end of the Middle Silurian. A back-arc basin developed between the Bainaimiao island arc belt and the North China craton, which consists of the Huangheshao syenites and Middle–Late Silurian Xuniwusu Formation (Fig. 7d).

(E) Early Silurian (~420 Ma): The subduction of the Wenduermiao oceanic plate terminated, which is followed by the collisional phase between Bainaimiao island arc and North China craton. The Xibiehe Formation was deposited as the back-arc basin closed (Fig. 7e).

Conclusions

Our new geochemical and geochronological analyses of the granitoids enable us to draw the following conclusions:

(1) We suggest the younger 422.5 ± 1.3 Ma age of Weijing pluton crystallization, older ages of 482.8 ± 3.5 Ma and 458.5 ± 2.8 Ma are interpreted to represent the ages of inherited zircon. The formation age of the Wenduermiao subduction–accretionary complex is suggested to be the Middle Cambrian–Late Silurian (509-421 Ma), which consists of the age of oceanic crust, different stages of arc magmatic rocks, and forearc sedimentary.

(2) We report the Bainaimiao granitoid with a weighted average $^{206}Pb/^{238}U$ age of 438.7 ± 1.8 Ma. The tectonic nature of the Bainaimiao island arc belt is continental marginal arc, and the time of activity could be in the Late Cambrian–Early Silurian (501–437 Ma). We suggested the existence of the back-arc basin between the Bainaimiao island arc belt and the North China craton. We obtain a U–Pb zircon age of the Huangheshao syenites of 433.8 ± 1.8 Ma, indicating that the back-arc basin has a formation age that is slightly later than the Bainaimiao island arc.

(3) The Wenduermiao subduction–accretionary complex could belong to the early oceanic crust and the Xilin-Hot microcontinental block, while the basement of the Bainaimiao island arc belt should be the North China craton. We suggest the existence of the Wenduermiao Ocean between the Wenduermiao subduction–accretionary complex and the Bainaimiao island arc belt during Early Paleozoic.

(4) We propose a model for the tectonic history and setting of these Early Paleozoic granitoids in central Inner Mongolia. We suggest that the tectonic evolution of study area during Early Paleozoic should be divided into five phases.

Acknowledgments We are grateful to Prof. Robert J. Stern for his help with the manuscript and extremely valuable comments. We thank Mr Andrew Zuza from the UCLA for his help on English polishing. We sincerely thank two anonymous reviewers for constructive and helpful reviews and Professor Wolf-Christian Dullo for comments and editorial handing. This work was financially supported by the Fundamental Research Funds for the Central Universities (2652013002) and the China Geological Survey Program (1212011220465; 12120114093901).

References

Andersen T (2002) Correction of common lead in U–Pb analyses that do not report204Pb. Chem Geol 192:59–79

Barbarin B (1999) A review of the relationships between granitoid types, their origins and their geodynamic environments. Lithos 46:605–626

Boynton WV (1984) Geochemistry of the rare-earth elements: meteorite studies. In: Henderson P (ed) Rare earth element geochemistry. Elsevier, Amsterdam, pp 63–114

Briggs SM, Yin A, Manning CE, Chen ZL, Wang XF (2009) Tectonic development of the southern Chinese Altai Range as determined by structural geology, thermobarometry, $^{40}Ar/^{39}Ar$ thermochronology, and Th/Pb ion-microprobe monazite geochronology. Geol Soc Am Bull 121:1381–1393

Bureau of Geology and Mineral Resources of Nei Mongol Autonomous Region (BGMRN) (1991) Regional geology of Inner Mongolia autonomous region. Geological Publishing House, Beijing, p 74 **(in Chinese)**

Chen B, Jahn BM, Wilde SA, Xu B (2000) Two contrasting Paleozoic magmatic belts in northern Inner Mongolia, China: petrogenesis and tectonic implications. Tectonophysics 328(1–2):157–182

De Jong K, Xiao WJ, Windley BF, Masago H, Lo CH (2006) Ordovician$^{40}Ar/^{39}Ar$ phengite ages from the blue schist-facies Ondor Sum subduction-accretion complex (Inner Mongolia) and implications for the Early Paleozoic history of continental blocks in China and adjacent areas. Am J Sci 306(12):799–845

Gao S, Rudnick RL, Xu WL, Yuan HL, Liu YS, Walker RJ, Puchtel IS, Liu XM, Huang H, Wang XR, Yang J (2008) Recycling deep cratonic lithosphere and generation of intraplate magmatism in the North China Craton. Earth Planet Sci Lett 270:41–53

Ge MC, Zhou WX, Yu Y, Sun JJ, Bao JQ, Wang SH (2011) Dissolution and supracrustal rocks dating of Xilin Gol Complex, Inner Mongolia, China. Earth Sci Front 18(5):182–195 **(in Chinese with English abstract)**

Gu CN, Zhou ZG, Zhang YK, Liu CF, Liu WC, Yu YS (2012) Zircon dating of the Baiyinduxi Group in Inner Mongolia and its tectonic interpretation. Geoscience 26(1):1–9 **(in Chinese with English abstract)**

Hsü KJ, Chen HL (1999) Geologic Atlas of China: an application of tectonic facies concept to the geology of China. Elsevier, Amsterdam

Hu X, Niu SY, Zhang YT (1987) The Middle-Late Silurian flysch in the Bainaimiao area, Nei Monggol. Reg Geol China 4:333–340

Hu X, Xu CS, Niu SY (1990) Evolution of the Early Paleozoic Continental Margin in Northern Margin of the North China Platform.

Beijing University Press, Beijing, pp 1–215 **(in Chinese with English abstract)**

Jahn BM, Windley B, Natal'in B, Dobretsov N (2004) Phanerozoic continental growth in Central Asia. J Asian Earth Sci 23:599–603

Jia HY, Bao Y, Zhang YQ (2003) Characteristics and tectonic significance of the Wude suture zone in northern Damaoqi, Inner Mongolia. J Chengdu Univ Technol 30(1):30–34 **(in Chinese with English abstract)**

Jian P, Liu DY, Kröner A, Windley BF, Shi YR, Zhang FQ, Shi GH, Miao LC, Zhang W, Zhang Q, Zhang LQ, Ren JS (2008) Timescale of an Early to Mid-Paleozoic orogenic cycle of the long lived Central Asian Orogenic Belt, Inner Mongolia of China: implications for continental growth. Lithos 101(3–4):233–259

Jian P, Liu DY, Kröner A, Windley BF, Shi YR, Zhang W, Zhang FQ, Shi GH, Miao LC, Zhang LQ, Tomurhuu D (2010) Evolution of a Permian intraoceanic arc–trench system in the Solonker suture zone, Central Asian Orogenic Belt, China and Mongolia. Lithos 118:169–190

Kheraskova TN, Didenko AN, Bush VA, Volozh YA (2003) The Vendian-Early Paleozoic history of the continental margin of Eastern Paleogondwana, Paleoasian Ocean, and Central Asian Foldbelt. Rus J Earth Sci 5:165–184

Kröner A, Kovach V, Belousova E, Hegner E, Armstrong R, Dolgopolova A, Seltmann R, Alexeiev DV, Hoffmann JE, Wong J, Sun M, Cai K, Wang T, Tong Y, Wilde SA, Degtyarev KE, Rytsk E (2014) Reassessment of continental growth during the accretionary history of the Central Asian Orogenic Belt. Gondwana Res 25(1):103–125

Le Maitre RW (1984) A proposal by the IUGS Subcommission on the systematics of igneous rocks for a chemical classification of volcanic rocks based on the total alkali silica (TAS) diagram. Aust J Earth Sci 31:243–255

Le Maitre RW (1989) A classification of igneous rock and a glossary of terms: rccommendations of the international union of geological science subcommision on the systematics of igneous rocks. Blackwell, Oxford, pp 1–193

Levashova NM, Van der Voo R, Abrajevitch AV, Bazhenov ML (2009) Paleomagnetism of mid-Paleozoic subduction-related volcanics from the Chingiz Range in NE Kazakhstan: the evolving paleogeography of the amalgamating Eurasian composite continent. Geol Soc Am Bull 121:555–573

Li SQ (1997) Early Paleozoic Era terrane pieced together and accreted in middle of Inner Mongolia. Geol Inner Mong 24:18–23 **(in Chinese with English abstract)**

Li HK, Geng JZ, Hao S, Zhang YQ, Li HM (2009) The study of zircon U–Pb dating by means LA–MC–ICPMS. Bull Mineral Petrol Geochem 28:77 **(supplement, in Chinese)**

Li CD, Ran H, Zhao LG, Wang HC, Zhang K, Xu YW, Gu YC, Zhang YQ (2012a) LA-MC-ICPMS U-Pb geochronology of zircons from the Wenduermiao Group and its tectonic significance. Acta Petrol Sin 28(11):3705–3714 **(in Chinese with English abstract)**

Li WB, Zhong RC, Xu C, Song B, Qu WJ (2012b) U-Pb and Re–Os geochronology of the Bainaimiao Cu–Mo–Au deposit, on the northern margin of the North China Craton, Central Asia Orogenic Belt: implications for ore genesis and geodynamic setting. Ore Geol Rev 48:139–150

Li YL, Zhou HW, Brouwer FM, Xiao WJ, Wijbrans JR, Zhong ZQ (2014) Early Paleozoic to Middle Triassic bivergent accretion in the Central Asian Orogenic Belt: insights from zircon U–Pb dating of ductile shear zones in central Inner Mongolia, China. Lithos 205:84–111

Liang Q, Grégoire DC (2000) Determination of trace elements in twenty six Chinese geochemistry reference materials by inductively coupled plasma-mass spectrometry. Geostand Newslett 24(1):51–63

Liu DY, Jian P, Zhang Q, Zhang F, Shi YR, Shi GH, Zhang NQ, Tao H (2003) SHRIMP dating of adakites in the Tulingkai ophiolite, Inner Mongolia: evidence for the Early Paleozoic subduction. Acta Geol Sin 77(3):317–327 **(in Chinese with English abstract)**

Liu JF, Chi XG, Zhang XZ, Ma ZH, Zhao Z (2009) Geochemical characteristic of Carboniferous quartz—diorite in the southern Xiwuqi area, Inner Mongolia and its tectonic significance. Acta Geol Sin 83(3):365–376 **(in Chinese with English abstract)**

Liu CF, Yang SS, Wu JW, Zhang HF (2010a) Dating and petrogenesis of late Permian-Early Triassic peraluminous granites in the Siziwangqi area, Inner Mongolia. Acta Geol Sin 84(7):1012–1016 **(in Chinese with English abstract)**

Liu CF, Zhang HR, Yu YS, Zhou ZG, Liu WC, Zhang HF (2010b) Dating and petrochemistry of the Beijige Pluton, Siziwangqi, Inner Mongolia. Geoscience 24(1):112–119 **(in Chinese with English abstract)**

Liu YS, Wang XH, Wang DB, He DT, Zong KQ, Gao CG, Hu ZC, Gong HJ (2012) Triassic high-Mg adakitic andesites from Linxi, Inner Mongolia: insights into the fate of the Paleo-Asian ocean crust and fossil slab-derived melt–peridotite interaction. Chem Geol 328:89–108

Liu CF, Liu WC, Zhou ZG (2014) Geochronology, Geochemistry and Tectonic setting of the Paleozoic-Early Mesozoic Intrusive in Siziwangqi, Inner Mongolia. Acta Geol Sin 88(6):992–1002 **(in Chinese with English Abstract)**

Liu CF, Wu C, Zhu Y, Zhou ZG, Jiang T, Liu WC, Li HY (2015) Late Paleozoic-Early Mesozoic magmatic history of the central Inner Mongolia, China: Implications for the Tectonic Evolution of the Xingmeng Orogenic Belt, southeastern segment of the Central Asian Orogenic Belt. J Asian Earth Sci. doi:10.1016/j.jseaes.2015.09.011

Ludwig KR (2003) User's manual for Isoplot 3.00: a geochronological toolkit for Microsoft Excel. Berkeley Geochronology Center Special Publication 4, 70 Berkeley, USA

Miao LC, Liu DY, Zhang FQ, Fan WM, Shi YR, Xie HQ (2007) Zircon SHRIMP U-Pb ages of the "Xinghuadukou Group" in Hanjiayuanzi and Xinlin areas and the "Zhalantun Group" in Inner Mongolia, Da Hinggan Mountains. Chin Sci Bull 52(8):1112–1134

Nie FJ, Pei RF, Wu LS, Bjorlykke A (1995) Nd and Sr isotopic study on greenschist and granodiorite of the Bainaimiao district, Inner Mongolia, China. Bull Chin Acad Geol Sci 1:36–44 **(in Chinese with English abstract)**

Pearce JA, Lippard SJ, Roberts S (1984) Characteristics and tectonic significance of supra-subduction zone ophiolites. In: Kokelaar BP, Howells MF (eds) Marginal basin geology, vol 16. Geological (London) Society Special Publication, pp 77–94

Rickwood PC (1989) Boundary lines within petrologic diagrams which use oxides of major and minor elements. Lithos 22:247–263

Şengör AMC, Natal'in BA (1996) Paleotectonics of Asia: fragments of a synthesis. In: Yin A, Harrison TM (eds) The tectonic evolution of Asia. Cambridge University Press, New York, pp 486–640

Sengör AMC, Natal'in BA, Burtman VS (1993) Evolution of the Altaid tectonic collage and Palaeozoic crustal growth in Eurasia. Nature 364:299–307

Shao JA (1991) Crust Evolution in the Middle Part of the Northern Margin of Sino-Korean Plate. Peking University Press, Beijing, pp 1–135 **(in Chinese)**

Shi YR, Liu GY, Zhang Q, Jian P, Zhang FQ, Miao LC, Shi GH, Zhang LQ, Tao H (2005) The petrogenesis and SHRIMP dating of the Baiyinbaolidao adakitic rocks in southern Suzuoqi, Inner Mongolia. Acta Petrol Sin 21(1):143–150 **(in Chinese with English abstract)**

Song B, Allen PN, Liu DY, Wu JS (1996) 3800 to 2500 Ma crustal evolution in the Anshan area of Liaoning Province, northeastern China. Precambr Res 78:79–94

Stern RJ (2002) Subduction zones. Rev Geophys 40:1–40

Stern RJ (2004) Subduction initiation: spontaneous and induced. Earth Planet Sci Lett 226:275–292

Streckeisen AL (1973) Plutonic rocks, classification and nomenclature recommended by the IUGS subcommission on the systematics of igneous rocks. Geotimes 18(10):26–30

Sun SS, Mcdonough WF (1989) Chemical and isotopic systematics of oceanic basalts: implications for mantle composition and processes. In: Saunders AD, Norry MJ (eds) Magmatism in the ocean basalts. Geological Society Special Publication, pp 313–345

Tang KD (1992) Tectonic evolution and minerogentic regularities of the fold Belt along the northern margins of Sino-Korean plate. Peking University Press, Beijing, pp 1–264 (**in Chinese with English abstract**)

Tang KD, Yan Z (1993) Regional metamorphism and tectonic evolution of the inner mongolia suture zone. J Metamorph Geol 11:511–522

Tang KD, Yan ZJ, Zhang RP (1983) On Wentermiao Group and its tectonic significance. In: Contributions for the project of plate tectonics in Northern China 1. Geological Publishing House, Beijing, pp 186–208 (**in Chinese with English abstract**)

Tong Y, Hong DW, Wang T, Shi XJ, Zhang JJ, Zeng T (2010) Spatial and temporal distribution of granitoids in the middle segment of the Sino-Mongolian border and its tectonic and metallogenic implications. Acta Geosci Sin 31(3):395–412 **(in Chinese with English abstract)**

von Raumer JF, Stampfli GM, Bussy F (2003) Gondwana-derived microcontinents—the constituents of the Variscan and Alpine collisional orogens. Tectonophysics 365:7–22

Wang B, Chen Y, Zhan S, Shu LS, Faure M, Cluzel D, Charvet J, Laurent-Charvet S (2007) Primary Carboniferous and Permian paleomagnetic results from Yili Block and their geodynamic implications on evolution of Chinese Tianshan Belt. Earth Planet Sci Lett 263:288–308

Whalen JB, Currie KL, Chappell BW (1987) A-type granites: geochemical characteristics, discrimination and petrogenesis. Contrib Mineral Petrol 95(4):407–419

Windley BF, Alexeiev D, Xiao WJ, Kröner A, Badarch G (2007) Tectonic models for accretion of the Central Asian Orogenic Belt. J Geol Soc Lond 164:31–47

Wu FY, Jahn BM, Wilde SA, Sun DY (2000) Phanerozoic continental crustal growth: U–Pb and Sr–Nd isotopic evidence from the granites in northeastern China. Tectonophysics 328:89–113

Wu FY, Sun DY, Li HM, Jahn BM, Wilde SA (2002) A-type granites in Northeastern China: age and geochemical constraints on their petrogenesis. Chem Geol 187:143–173

Wu FY, Jahn BM, Wilde SA, Lo CH, Yui TF, Lin Q, Ge WC, Sun DY (2003a) Highly fractionated I-type granites in NE China (I): geochronology and petrogenesis. Lithos 66:241–273

Wu FY, Jahn BM, Wilde SA, Lo CH, Yui TF, Lin Q, Ge WC, Sun DY (2003b) Highly fractionated I-type granites in NE China (II): isotopic geochemistry and implications for crustal growth in the Phanerozoic. Lithos 67:191–204

Wu C, Jiang T, Liu CF, Liu WC (2014) Early Cretaceous A-type granites and Mo mineralization, Aershan area, eastern Inner Mongolia, Northeastern China: Geochemical and Isotopic constraints. Int Geol Rev 56(11):1357–1376

Wu C, Jiang T, Liu WC, Zhang D, Zhou ZG (2015) Early Cretaceous adakitic granites and mineralization of the Yili porphyry Mo deposit in the Great Xing'an Range: implications for the geodynamic evolution of northeastern China. Int Geol Rev 57(9–10):1152–1171

Xiao WJ, Windley BF, Hao J, Zhai MG (2003) Accretion leading to collision and the Permian Solonker suture, Inner Mongolia, China: termination of the central Asian orogenic belt. Tectonics 22:1484–1505

Xiao WJ, Windley BF, Huang BC, Han CM, Yuan C, Chen HL, Sun M, Sun S, Li JL (2009) End-Permian to Early-Triassic termination of the accretionary processes of the southern Altaids: implications for the geodynamic evolution, Phanerozoic continental growth, and metallogeny of Central Asia. Int J Earth Sci 98:1189–1217

Xiao WJ, Huang BC, Han CM, Sun S, Li JL (2010) A review of the western part of the Altaids: a key to understanding the architecture of accretionary orogens. Gondwana Res 18:253–273

Xiao WJ, Windley BF, Allen MB, Han CM (2013) Paleozoic multiple accretionary and collisional tectonics of the Chinese Tianshan orogenic collage. Gondwana Res 23:1316–1341

Xu B, Chen B, Zhang C, Bai ZQ (1994) The age and tectonic significance of ferrian metamorphic series in the middle segment of the North Margin of the North China Plate. Geol Rev 40(4):307–311 **(in Chinese with English abstract)**

Xu B, Charvet J, Chen Y, Zhao P, Shi GZ (2013) Middle Paleozoic convergent orogenic belts in western Inner Mongolia (China): framework, kinematics, geochronology and implications for tectonic evolution of the Central Asian Orogenic Belt. Gondwana Res 23(4):1342–1364

Yan GH, Mu BL, Xu BL, He GY, Tan LK, Zhao H, He ZF, Zhang RY, Qiao GS (1999) Triassic alkaline intrusive in the Yanliao-Yinshan area: their chronology, Sr, Nd and Pb isotopic characteristics and their implication. Sci China D 42(6):582–587

Ye M, Zhang SH, Wu FY (1994) The classification of the Paleozoic tectonic units in the area crossed by Manzhouli–Suifenghe geoscience transect. J Chang Univ 24:241–245 **(in Chinese with English abstract)**

Zhai MG, Santosh M (2011) The early Precambrian odyssey of the North China Craton: a synoptic overview. Gondwana Res 1:6–25

Zhang W, Jian P (2008) SHRIMP Dating of Early Paleozoic Granites from North Damaoqi, Inner Mongolia. Acta Geol Sin 82(6):778–787 **(in Chinese with English abstract)**

Zhang C, Wu TR (1999a) Features and tectonic implications of the ophiolitic mélange in the southern Suzuoqi, Inner Mongolia. Sci Geol Sin 34(3):381–389 **(in Chinese with English abstract)**

Zhang C, Wu TR (1999b) Rocks assemblage of Baiyinduxi Group and its tectonic interpretation in Boin Sum region, Inner Mongolia. Geol J China Univ 5(2):175–182 **(in Chinese with English abstract)**

Zhang HF, Zhou ZG, Liu WC, Li ZZ, Zhang YM, Liu CF (2009a) Grenvilltectono-thermal event record in the Bainaimiao area, Inner Mongolia, China: evidence from zircon LA-ICP-MA U-Pb dating of quart monzodiorite dike. Acta Petrol Sin 25(6):1512–1518 **(in Chinese with English abstract)**

Zhang SH, Zhao Y, Kröner A, Liu XM, Xie LW, Chen FK (2009b) Early Permian plutons from the northern North China Block: constraints on continental arc evolution and convergent margin magmatism related to the Central Asian Orogenic Belt. Int J Earth Sci 98:1441–1467

Zhang YM, Zhang HF, Liu WC, Zhou ZG (2009c) Timing and petrogenesis of the Damiao granodiorite, Siziwangqi, Inner Mongolia. Acta Petrol Sin 25(12):3165–3181 **(in Chinese with English abstract)**

Zhang XH, Zhang HF, Jiang N, Zhai MG, Zhang YB (2010) Early Devonian alkaline intrusive complex from the northern North China Craton: a petrological monitor of post-collisional tectonics. J Geol Soc Lond 167:717–730

Zhang W, Jian P, Kröner A, Shi YR (2013) Magmatic and metamorphic development of an early to mid-Paleozoic continental

margin arc in the southernmost Central Asian Orogenic Belt, Inner Mongolia, China. J Asian Earth Sci 72:63–74

Zhang SH, Zhao Y, Ye H, Liu JM, Hu ZC (2014) Origin and evolution of the Bainaimiao arc belt: implications for crustal growth in the southern Central Asian orogenic belt. GSA Bull 126:1275–1300

Zhou HP, Nie FJ, Xue FL (1992) Baiyinduxi Group, Bainaimiao Group and Baiyinduxi-Bainaimiao Terrane. J Chang Univ Earth Sci 22:17–28 **(Special Issue for the Bainaimiao Geology, in Chinese)**

Zhou ZG, Zhang HF, Liu HL, Liu CF, Liu WC (2009) Zircon U–Pb dating of basic intrusions in Siziwangqi area middle Inner Mongolia, China. Acta Petrol Sin 25(6):1519–1528 **(in Chinese with English abstract)**

Zonenshain LP, Kuz'min MI, Natapov LM (1990) Plate tectonics of the USSR territory. Nedra, Moscow, pp 1–327